Environmental Science & Technology

pubs.acs.org/est

Critical Review

Electrocatalytic Utilization of Air Pollutants and GHGs: Fundamentals, Electrode Materials, and Reactors

Liu Huang, Ziyan Fu, Haoyu Yin, Chuan Xia, Shuang Cao, Xiaole Weng, Le Shi,* and Zhongbiao Wu*

Cite This: *Environ. Sci. Technol.* 2025, 59, 24177−24196

Read Online

ACCESS | Metrics & More | Article Recommendations | Supporting Information

ABSTRACT: Air pollutants and greenhouse gases (GHGs) pose threats to the sustainable development of human society and ecosystems. While various established techniques are available for reducing air pollutant and GHG emissions from industrial sources, they typically focus on pollutant treatment rather than conversion and utilization. Electrocatalysis is a promising technology for converting these harmful gases into valuable chemicals using renewable energy inputs under mild conditions. Air pollutants and GHGs always coexist industrially and share some similar properties. Their electrochemical conversion, which occurs through similar electron-transfer mechanisms, can therefore be achieved synergistically in a specific scenario. This review critically examines the rationality, key considerations, and practical strategies for the synergistic conversion of air pollutants and GHGs, bridging the gap between laboratory research and industrial adoption. We assess the current state of electrocatalytic technologies, covering fundamental mechanisms, electrode materials, and reactor designs. Detailed analyses of electrocatalysts for anodic, cathodic, and synergistic reactions are provided along with investigations into reactor configurations and the role of external fields in enhancing performance. By exploring the challenges and future perspectives in gas-involved electrocatalysis, this review identifies critical barriers that need to be overcome to enable large-scale industrial implementation.

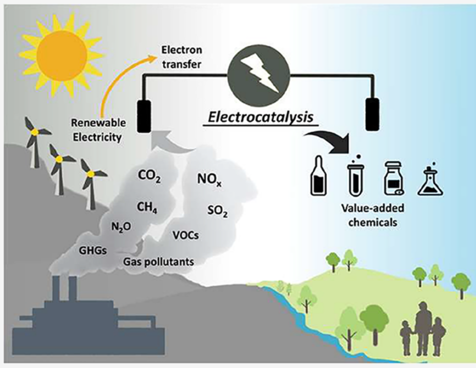

KEYWORDS: *climate change, air pollutants, greenhouse gases, mass transfer, synergistic reaction, industrial implementation*

1. INTRODUCTION

The rising concentrations of air pollutants and greenhouse gases (GHGs) pose significant threats to human health and environmental sustainability, driven by their interconnected origins and compounding impacts.[1] Air pollutants, such as sulfur dioxide (SO_2), nitrogen oxides (NO_x), and volatile organic compounds (VOCs), cause numerous environmental problems such as acid rain and soil acidification, with cascading effects on public health.[2,3] Concurrently, GHGs such as carbon dioxide (CO_2), methane (CH_4), and nitrous oxide (N_2O) drive global warming through atmospheric heat retention.[4] Their point-source emissions frequently coexist in highly energy-consuming sectors and share similar properties.[5] This overlap creates opportunities for synergistic migration strategies that offer both environmental and economic benefits.

Catalytic techniques are effective in converting these harmful gases into value-added chemicals. For example, CO_2 and CH_4 can be transformed into C_1/C_2 chemicals, such as methanol (CH_3OH) and ethanol (CH_3CH_2OH), while NO can be reduced to ammonia (NH_3). Among various catalytic technologies, such as thermal, photo, and electrocatalysis (Figure 1), electrocatalysis stands out as a sustainable alternative playing a crucial role in air pollutants and GHGs utilization by lowering activation energy and accelerating reaction rates. Especially, electrocatalysis is a future-oriented technology. By operating under mild conditions and utilizing renewable energy (e.g., solar and wind), electrocatalysis bypasses fossil fuel reliance while enabling precise control over reaction pathways through tunable potentials.[6,7] Their modular design also allows deployment in remote settings, such as offshore platforms and landfills, without complex and centralized infrastructure.[8] The electrocatalytic system also shows an economic promise that the production costs of carbon monoxide and formic acid (C_1 products) in the electrocatalytic CO_2 reduction reaction (CO_2RR) are approaching \$0.44 kg^{-1} and \$0.59 kg^{-1}, respectively, competitive with conventional processes.[9]

Synergistic electrocatalytic conversion of coexisting air pollutants and GHGs enhances efficiency, reduces energy demands, and mitigates cross-interference issues. Their shared electron-transfer mechanisms enable simultaneous processing

Received: May 17, 2025
Revised: October 10, 2025
Accepted: October 13, 2025
Published: October 27, 2025

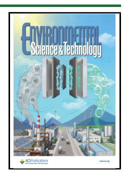

https://doi.org/10.1021/acs.est.5c06634
Environ. Sci. Technol. 2025, 59, 24177−24196

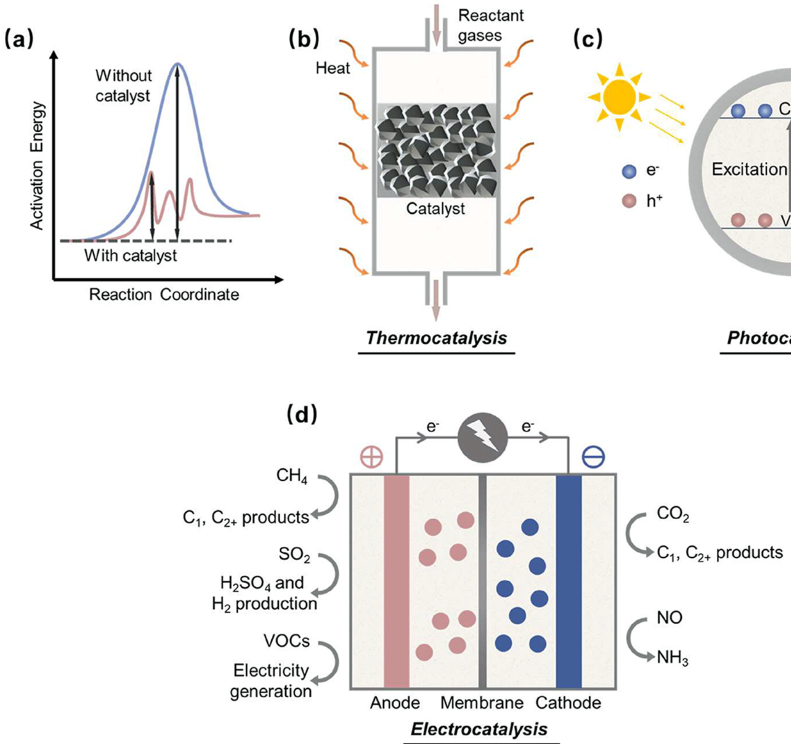

Figure 1. Mechanisms of (a) the change of free energy from without catalyst to with catalyst, (b) thermocatalysis, (c) photocatalysis, and (d) electrocatalysis.

of mixed gases under optimized conditions. For example, natural gas rich in CH_4 and CO_2 can be coprocessed, with multiple-gas systems achieving higher product yields and energy efficiency (EE) than single-gas systems.[10] This integration not only replaces fossil-fuel-driven treatments but also addresses secondary issues like energy-intensive steam methane reforming, which directly exacerbates CO_2 emissions.

Herein, given the coexistence of industrial pollutant gases and similar electrocatalytic reaction mechanisms, this review expands the electrocatalytic systems to under-reviewed air pollutants (NO_x, SO_2, and VOCs) and GHGs (CO_2, CH_4, and N_2O), with emphasis on their utilization and synergistic reactions. We analyze active species mechanisms during electrocatalysis and evaluate state-of-the-art electrocatalysts for anodic, cathodic, and coupled reactions. Reactor engineering strategies, including cell configurations and the coupling of external fields (e.g., photo-, thermo-, and magnetic fields), are explored for further improving the EE. To simultaneously address multiple pollutants, synergistic conversion pathways are systematically analyzed. Finally, we identify critical barriers hindering industrial adoption, proposing pathways to bridge the gap between laboratory research and scalable implementation.

2. ACTIVE SPECIES IN ELECTROCATALYTIC AIR POLLUTANTS AND GHG UTILIZATION

During electrocatalytic reactions, various active species are generated to interact with specific gases, playing a key role in governing the reaction pathways. The electrocatalytic oxidation process involves both direct and indirect pathways. Gas molecules can directly lose electrons upon adsorption on the active sites of electrocatalysts, or undergo indirect oxidation through charge and proton transfer mediated by oxidative agents such as radicals and high-valent metal ions (Figure 2a). For example, in electrochemical CH_4 oxidation reaction

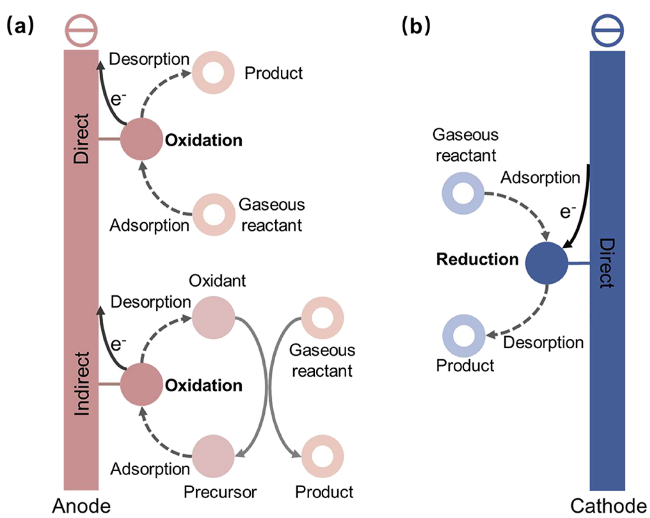

Figure 2. Electron transfer mechanisms in electrocatalytic systems: (a) direct and indirect pathways on the anode and (b) direct pathways on the cathode.

(CH_4OR), CH_4 can directly undergo dehydrogenation to form $*CH_3$ at the anodic active site.[11,12] Alternatively, C−H cleavage can be mediated by reactive oxygen species (ROS) (e.g., $*O$, $*OH$, and O^{2-}), chlorine intermidiate ($*Cl$), as well as high-valent metal ions (e.g., V^V, Pt^{IV}, and Pd^{III}).[13−15] These active species can be generated in the anode, including $*O$ (deriving from the oxidation of H_2O or CO_3^{2-}), $*Cl$ (deriving from the oxidation of Cl^-), and high-valent metal ions.[16] To enhance CH_4 oxidation efficiency, a strategic approach involves

https://doi.org/10.1021/acs.est.5c06634
Environ. Sci. Technol. 2025, 59, 24177−24196

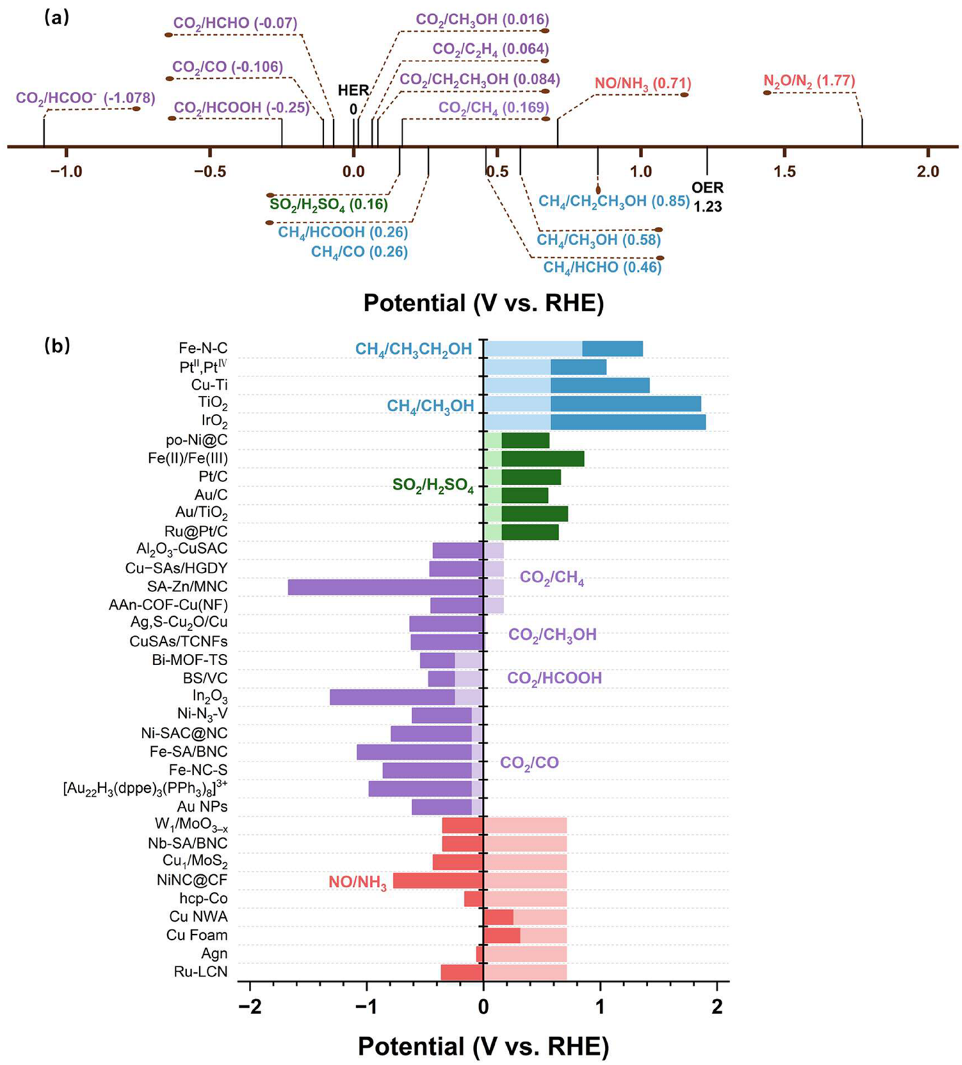

Figure 3. (a) Electrochemical oxidation/reduction potential of reactions involving CH_4,[205] SO_2,[34] CO_2,[206] NO,[22] and N_2O.[207] (b) Overpotential of different catalysts at 1 mA cm^{-2} (CH_4), or at 20 mA cm^{-2} (involving SO_2, CO_2, and NO) (see Table S1 in Supporting Information for details).

utilizing oxygen evolution reaction (OER) catalysts while optimizing the applied potential to stabilize *O and suppressing competing O_2 production.[13] Recent studies also propose utilizing active species reduced from O_2 or CO_2 (e.g., H_2O_2, O_2^-, or HOO^-) to facilitate CH_4OR near the cathode, thereby mitigating anodic overoxidation issues.[17,18] Similarly, in the electrochemical SO_2 oxidation reaction (SO_2OR), both direct electron transfer at the electrocatalyst active sites and radicals like *OH contribute to the oxidation mechanism.[19] In electrochemical VOCs treatment, organic pollutants can be selectively oxidized by electrode active sites or react with in situ-generated oxidizing agents (*OH, H_2O_2, O_3, ClO^-, and ClO_2^-) from the supporting electrolyte.[20]

In contrast, reduction reactions involving CO_2 or NO typically proceed through direct multielectron transfers without requiring external reductants or intermediates (Figure 2b). For CO_2 reduction, the reaction progresses through partial reduction to C_1 products like CO, HCOOH, and CH_3OH before undergoing complete reduction to CH_4 via an $8e^-/8H^+$ pathway.[21] The selectivity of these reactions is inherently challenging due to competing pathways requiring 2−12 electrons, which can yield diverse C_1 or C_{2+} products. Similarly, the electrochemical reduction of NO to NH_3 experiences a $5e^-/5H^+$ mechanism, proceeding via either a dissociative or associative pathway.[22] In the dissociative pathway, the N−O bond breaks on the active site, followed by independent hydrogenation of the adsorbed *N or *O species to produce NH_3 and H_2O. In contrast, the associative pathway involves sequential protonation of N and O atoms in the NO molecule, forming an intermediate (H_xNOH_y) that ultimately converts to NH_3.

3. ELECTROCHEMICAL REACTION PROCESS IN AIR POLLUTANTS AND GHG UTILIZATION

Electrochemical oxidation of CH_4, SO_2, and VOCs typically occurs at the anode, while CO_2 and NO_x undergo cathodic reduction. The selectivity of these reactions can be controlled by tailoring the catalyst design and tuning the applied potential. The thermodynamic oxidation and reduction potentials of these reactions vary significantly (Figure 3a), and the overpotential for representative catalysts reported in literature is intuitively compared (Figure 3b). The corresponding data of overpotential, current density, faradic efficiency (FE), and stability metrics are given in Table S1. Different factors, such as electronic structure, surface modification strategies, and electrolyte composition, will be systematically

https://doi.org/10.1021/acs.est.5c06634
Environ. Sci. Technol. 2025, 59, 24177−24196

analyzed to elucidate their impacts on activity and selectivity, aiming to advance the rational design of electrocatalysts for synergistic reaction systems.

3.1. Anodic Reaction.

3.1.1. CH_4 Conversion into C_1, C_{2+} Substances. CH_4, the cleanest and most abundant natural carbon resource, is widely distributed in natural gas, shale gas, coal-bed methane, and methane hydrates. Efficient on-site conversion of CH_4 into transportable, high-value-added chemicals holds important economic and environmental benefits. However, the CH_4 molecule's high tetrahedral symmetry and strong C−H bond (bond energy: 439.3 kJ/mol) require harsh conversion conditions. Industrial processes like steam reforming/Fischer-Tropsch synthesis convert CH_4 into syngas (CO/H_2), featuring a high energy intensity and large CO_2 emissions. Direct catalytic oxidation of CH_4 to high-value-added chemicals under mild conditions presents a major challenge in fields of catalysis and chemical engineering, often regarded as a "holy grail" problem.

Transition metal oxide (TMO) catalysts have the potential to electrochemically oxidize CH_4 into CH_3OH. The CH_4OR activity of TMOs is determined by both higher CH_4 binding energy and lower Madelung potential of the metal in TMOs, and efficient activation of the C−H bond occurs at the stable O active sites on top of the metal in TMOs.[23] An investigation of CH_4 adsorption on 12 TMOs revealed that the reaction pathway is potential-dependent: $^*CH_x$ intermediates dominate at lower potentials, while $^*CH_3OH$ becomes the primary intermediate at higher potentials. To mitigate $^*CH_3OH$ overoxidation, Cu−Ti bimetallic catalysts were developed, where Cu sites promoted $^*CH_3$−$^*OH$ coupling and facilitated $^*CH_3OH$ desorption.[24]

Interface engineering based on TMOs has proven to be effective in facilitating CH_4 oxidation to ethanol. For example, a catalyst containing 3% Ni transformed into NiO after calcination, exhibiting optimized interfacial properties that promote efficient C−H activation and C−C coupling.[25] The NiO(200)/Ni(111) interface significantly reduced activation energy barriers compared to pure Ni, resulting in a remarkable 89% ethanol FE and a yield of 25 μmol g_{cat}^{-1} h^{-1} at 1.40 V vs RHE. Cocatalyst integration further exemplifies this strategy, where distinct components synergistically drive reaction steps. In Rh/ZnO nanosheets, Rh stabilized $^*CH_3$ species from CH_4, while ZnO facilitated water oxidation to *O, achieving an ethanol yield of 789 μmol g_{cat}^{-1} h^{-1} at 2.2 V vs RHE.[26]

Rational design of TMO composites is a promising approach for generating C_3 liquid fuels in CH_4OR. For example, a Co_3O_4/ZrO_2 nanocomposite exhibited high efficiency in the electrochemical oxidation of CH_4 to 2-propanol and 1-propanol using carbonate electrolyte, where ZrO_2 acted as both a structural support and an oxidant source.[27] The overall production efficiency reached 60%, showcasing the potential for practical CH_4 conversion under ambient conditions. Subsequently, a ZrO_2:$NiCo_2O_4$ quasi-solid solution catalyst with the ability to form stable CH_3O species could enable partial CH_4 conversion into oxygenates, including propionic acid, acetic acid, and acetone.[28]

Electrocatalysts in the electrolyte, such as metal species with high redox potentials, could convert CH_4 more rapidly with high FE, and functionalize CH_4 with some specific groups. For example, a Pt^{II}-containing electrolyte enabled continuous regeneration of Pt^{IV}, a stronger oxidant in CH_4 oxidation.[15] By employing Cl-adsorbed Pt electrodes, Pt^{II} could be facilely oxidized to Pt^{IV} with a remarkable 70% selectivity for CH_3OH at low overpotentials. During the electrochemical oxidation of Pd^{II} salts in concentrated sulfuric acid, a $Pd_2^{III,III}$ intermediate assisted CH_4 activation, yielding CH_3OSO_3H and CH_3SO_3H through both faradaic and nonfaradaic pathways.[29] Additionally, a vanadium(V)-oxo dimer electrocatalyst could oxidize CH_4 to CH_3OSO_3H with a low activation barrier and a high turnover frequency (TOF).[12] This system converted natural gas mixtures into liquid products with 90% FE and turnover numbers exceeding 100,000 over 240 h, highlighting its potential for decentralized applications requiring minimal upstream separation or centralized infrastructure.

3.1.2. SO_2 Oxidation along with H_2 Production. SO_2, a toxic pollutant, also exhibits potential for industrial hydrogen production through electrolysis in aqueous media. SO_2OR theoretical potential of only 0.158 V vs SHE at the anode,[30] making it more energy-efficient than OER (E° = 1.23 V vs SHE) in water electrolysis.[31] This principle underpins prominent sulfur-based hydrogen cycles, including the hybrid sulfur (HyS) cycle and the sulfur-iodine (SI) cycle.[30] The SI cycle features an electrochemical Bunsen reaction, avoiding the need for excess iodine and water, operating through two key electrode reactions:[32]

$$\text{Anodic reaction } SO_2 + 2H_2O - 2e^- \rightarrow H_2SO_4 + 2H^+ \quad (1)$$

$$\text{Cathodic reaction } I_2 + 2H^+ + 2e^- \rightarrow 2HI \quad (2)$$

$$\text{Overall reaction } SO_2 + I_2 + 2H_2O \rightarrow H_2SO_4 + 2HI \quad (3)$$

In the SI cycle, HI is decomposed into H_2 and I_2, while H_2SO_4 is concentrated or decomposed, thereby closing the loop. In contrast, the HyS cycle can achieve an EE of up to 48−50%.[30,33] The anodic reaction involves the oxidation of SO_2 to H_2SO_4, while H^+ is directly reduced to H_2 at the cathode. Both cycles leverage the SO_2OR for hydrogen production, indirectly in the SI cycle and directly in the HyS cycle.

The electrochemical SO_2OR has mainly focused on Pt-based catalysts. For instance, in a Ru@Pt core-shell nanostructure, the incorporation of Ru modified the Pt crystal lattice parameters and induced an electronic effect on Pt atoms, assisting H_2O activation and enhancing adsorption ability.[19] Catalytic activity was directly linked to the magnitude of this electronic effect, with cyclic voltammetry (CV) confirming the presence of adsorbed *OH intermediates. Comparative analysis of alloy and core-shell structures revealed that both structures improved performance via electronic and bifunctional effects, but the Ru@Pt/C core-shell structure outperformed alloys due to better Pt utilization and long-term stability.[34] Similarly, acid-treated Pt_xNi_y/C (with a Pt-rich surface) exhibited compressed Pt lattices and increased valence electron vacancies.[30] Among these, Pt_1Ni_3/C exhibited the highest catalytic activity, showing a current density nearly 80% higher than that of the commercial Pt/C catalyst, attributed to its optimized electronic structure and enhanced Pt accessibility.

The preparation of Pt-based catalysts, including support selection and deposition techniques, critically influences Pt loading and catalytic performance. While higher Pt loadings enhance electrolysis efficiency, achieving optimal activity with loadings exceeding 40% remains challenging due to particle aggregation and uneven distribution.[32] Strategic support

https://doi.org/10.1021/acs.est.5c06634
Environ. Sci. Technol. 2025, 59, 24177−24196

materials, such as reduced graphene oxide (rGO)/carbon black (CB) composite-supported Pt (Pt/GC), enabled high Pt loading while maintaining a small size, uniformly dispersed Pt nanoparticles.[32] Deposition techniques also have a significant influence on catalyst activity and stability.[35] For instance, the electrospray (ES) method outperforms conventional air gun (AG) deposition by achieving uniform catalyst distribution on the gas diffusion layer (GDL) with a broad Pt loading range (0.025−0.3 mg_{Pt} cm^{-2}). Electrodes with lower Pt loadings using the ES method demonstrated enhanced electrochemical surface area (ECSA), and higher activity and stability in the SO_2OR.

Au has emerged as a high-performance catalyst in SO_2OR.[36] Carbon-supported Au (Au/C) exhibited an earlier onset potential than Pt/C in low-concentration sulfuric acid and a higher TOF at higher acid concentrations.[36] In situ electrolysis with low Au loadings further displayed higher current densities and greater stability than Pt. To address noble metals' scarcity, nanostructured strategies such as Au supported on TiO_2 (Au/TiO_2) reduced catalyst mass while enhancing activity beyond bulk Au.[31] Additionally, non-noble-metal-based catalysts, such as partially oxidized Ni@C (po-Ni@C), also showed stability in acidic solutions and even outperformed the 20% Pt/C catalyst.[37]

Electrolyte composition is also effective at minimizing SO_2OR impedance. For instance, iodide additives, particularly hydroiodic acid (HI) in the anolyte, lowered overpotentials and enhanced reaction kinetics.[38] Similarly, integrating a Fe(II)/Fe(III) redox cycle facilitated the HyS cycle using $FeCl_3$ as the oxidant and Ar plasma-treated carbon paper (A-CP) as the anode.[39] This SO_2-assisted Fe(II)/Fe(III) system, coupled with the hydrogen evolution reaction (HER), achieved an ultralow cell voltage of 0.97 V at 10 mA cm^{-2} compared to conventional water electrolysis (1.85 V), by leveraging the low oxidation potentials of Fe^{2+} and SO_2. Such innovations highlight the promise of energy-efficient hydrogen production and SO_2 remediation in industrial settings.

3.1.3. VOC Degradation and Utilization. VOCs emitted from exhaust gases, waste incineration, fuel refining, and chemical manufacturing pose significant environmental and health risks.[40] Their removal strategies involve either direct gas-phase degradation or indirect liquid-phase transfer and oxidation. For persistent VOCs like toluene and chlorobenzene, investigated approaches combining absorption with oxidation have been widely explored.[20,41−43] The initial absorption of VOCs is crucial in the overall removal process, influenced by the intrinsic wettability, solvent properties, reactor configuration, mass transfer kinetics, and presence of oxidizing agents in the solvent. Electrochemical oxidation stands out as a sustainable method, generating reactive species to degrade absorbed VOCs without secondary pollution.

In electrochemical VOC destruction systems, the absorbent and electrolyte are usually the same solvent. Ionic liquids, for instance, have been utilized as both an absorbent and electrolyte in degrading ethanethiol and thiophene.[44,45] While fluorine-modified β-PbO_2 electrodes enhanced degradation via *OH generation, achieving full mineralization remained elusive. Optimizing reactor designs also contributes to enhancing performance. For example, a stacked-mesh electrochemical absorber with five electrode pairs maximized styrene removal by tuning electrode dimensions and spacing.[46] Similarly, a Venturi-based jet electrode-absorber controlled perchloroethylene degradation pathways by regulating bubble size through throat width adjustments.[47]

Although complete VOC mineralization remains challenging, their chemical energy can be used for electricity generation. A notable advancement is the use of toluene as an anodic fuel in a solid oxide fuel cell (SOFC) with a yttrium-stabilized zirconia (Ni-YSZ) anode and fused $Ce_xGd_yO_z$ electrolyte.[48] Operating at 600 °C, this system achieved 94.19% toluene removal efficiency even at extreme concentrations (1.874×10^5 ppmv) while generating 14 mW cm^{-2} of power, demonstrating the viability of simultaneous VOCs abatement and energy conversion.

3.2. Cathodic Reaction. *3.2.1. CO_2 Conversion into C_1, C_{2+} Substances.* Electrochemical conversion of CO_2 into value-added chemicals mitigates the greenhouse effect and generates economic value, although it presents several challenges. The high C=O bond energy requires substantial overpotentials (hundreds of millivolts) to drive reduction. Effective electrocatalyst design requires a deep understanding of reaction thermodynamics and kinetics to promote CO_2 reduction while suppressing the competing HER. Achieving high selectivity remains challenging due to the diverse pathways of CO_2RR, which yield diverse products ranging from C_1 species (CO, HCHO, HCOOH, CH_3OH, and CH_4) to C_2 compounds (C_2H_4, CH_3CHO, and C_2H_5OH) via 2−12 electron transfer.[49]

The CO_2RR mechanism initiates with the rate-limiting CO_2 activation to form $*CO_2^-$ intermediates. Subsequent protonation pathways bifurcate based on the adsorption of $*CO_2^-$: protonation at the carbon atom yields *OCHO, favoring HOOH or $HCOO^-$ formation; while oxygen atom protonation forms *COOH, leading to the generation of *CO. The selectivity of the CO_2RR depends on the relative binding strengths of key intermediates (*OCHO, *COOH, *CO, and *H). Weak *CO adsorption promotes CO production, whereas strong *CO binding enables further reduction to hydrocarbons (e.g., CH_4 and C_2H_4) or alcohols (e.g., CH_3OH, C_2H_5OH) through C−C coupling or multistep proton-electron transfers.[50]

The selective production of C_1 and C_2 products in the CO_2RR can be achieved by tailoring applied potentials and electrocatalyst design. For C_1 products, CO is a prominent target formed through a two-electron transfer process, which has been extensively studied using noble metals such as Au, Ag, and Pt. Monodisperse Au nanoparticles demonstrate notable activity and selectivity, although their surface structure-property relationships remain a challenge.[51,52] Recent advances highlight atomically precise Au nanoclusters, such as the $[Au_{22}H_3(dppe)_3(PPh_3)_8]^{3+}$, which features a unique $Au_{22}H_3$ core with three bridging H atoms.[53] This catalyst exhibited a 92.7% FE at −0.6 V vs RHE and a high reaction activity of 134 mA $mg^{-1}{}_{Au}$ over 10 h. In contrast, Ag catalysts offer a cost-effective alternative for CO formation, combining scalability with high selectivity.[54] For instance, Ag nanoparticles modified with redox-active CO_2 sorbents reach steady CO FEs > 90% at 1200 mA cm^{-2} with a notable mass activity of 174 A $mg^{-1}{}_{Ag}$.[55]

Recently, single atom catalysts (SACs) with isolated active sites have demonstrated exceptional electrocatalytic activities in CO_2 reduction to various products with the ability to inhibit *H combination within competitive HER.[56−60] For example, in terms of CO generation, a Co SAC with Co−N_5 coordination achieves >99.2% FE_{CO} and extraordinary stability by promoting CO_2 activation, rapid formation of *COOH, and

https://doi.org/10.1021/acs.est.5c06634
Environ. Sci. Technol. 2025, 59, 24177−24196

efficient CO desorption.[59] Similarly, a Ni SAC achieves a high FE_{CO} of 95% at −0.6 V vs RHE while resisting metal aggregation.[58] Beyond traditional metals, erbium (Er) SACs set a record high TOF of ∼130,000 h^{-1} at 500 mA cm^{-2},[60] outperforming Ni−N_3O SACs (TOF of 135,000 h^{-1} at only 65 mA cm^{-2}).[61] These high TOFs correlated with high EE and CO_2 conversion efficiency. Notably, kilogram-scale synthesis of carbon-supported SACs with high metal loadings has been realized, making a critical step toward industrial adoption.[62]

HCOOH/$HCOO^-$, valuable two-electron CO_2RR products, are highly desirable for their easy collection, low toxicity, and industrial versatility.[54,63] P-block metals (In, Sn, Pb, Bi, and Sb) effectively convert CO_2 to $HCOO^-$ or HCOOH by generating the intermediate *OCHO.[64,65] With the exclusive $Sb^{\delta+}$−N_4 ($0 < \delta < 3$) active sites while suppressing HER, a Sb SAC on N-doped carbon matrix showed a high $HCOO^-$ FE of 94.0% at −0.8 V vs RHE.[66] Similarly, sulfur-doped Zn-Sn dual-atom catalyst with p-d coupling effect showed 94.6% FE at −0.90 V.[67] Carbon-coated tip-like In_2O_3 exhibited an extraordinary HCOOH FE of 98.9% at 300 mA cm^{-2} and >100 h stability in low-K^+ acidic electrolyte.[68] Scaling to a 25 cm^2 electrolyzer yielded a 7 A total current with stable HCOOH production, highlighting industrial feasibility. Among p-block metals, Bibased catalysts (metallic Bi, BiO_x, $BiPO_4$, $Bi_2O_2CO_3$, and Bi_2S_3) exhibit optimal *OCH binding for formate selectivity.[69−75] To prevent active defect sites from hydroxyl poisoning, vitamin C-modified Bi_3S_2 achieved stable pure HCOOH production over 120 h in a solid-electrolyte reactor.[74] Tensile-strained Bi-MOF-TS catalyst further activated inert Bi sites, showing a record HCOOH partial current density of −995 ± 93 mA cm^{-2} with high FE and CO_2 conversion efficiency.[76]

CH_3OH is a six-electron CO_2RR product serving as a liquid fuel and energy carrier. While noble metals (Ru, Pt, and Pb) have been explored,[77−79] Cu-based catalysts dominate due to low cost and high performance.[80] Copper selenide nanocatalysts exhibited 77.6% FE at 41.5 mA cm^{-2} with an overpotential of 285 mV.[81] Atomically dispersed Cu SAs on through-hole carbon nanofibers (TCNFs), exhibiting a 44% FE and a partial current density of 93 mA cm^{-2} for CH_3OH.[80] Ag-doped Cu_2O/Cu heterostructures enhanced selectivity by stabilizing *CHO intermediates and suppressing HER, achieving 67.4% FE and 122.7 mA cm^{-2} current density.[82]

As a C_1 product of the eight-electron CO_2RR, CH_4 is highly valued for its energy density (55.5 GJ/ton), compatibility with existing infrastructure, and potential to replace fossil fuels. Cu-based materials are widely investigated for CH_4 production.[83] For example, anthraquinone-based covalent organic frameworks (COFs) functionalized with Cu achieved a FE_{CH4} of 77% at 128.1 mA cm^{-2}, leveraging their tunable 1D superstructures.[75] Similarly, low-coordinated Cu clusters decorated by Cu−N/O single sites achieved a FE_{CH4} of 71% with less than 3% CO_2 loss at 100 mA cm^{-2} while halving energy consumption (254 GJ/ton CH_4) compared to conventional methods.[84] With low coordination Cu−C_2 sites promoting *H production, Cu SAC achieved a selectivity of 72.1% and a high CH_4 partial current density of 230.7 mA cm^{-2}.[85] Metal-support interactions further modulate Cu electronic structures to form different highest occupied orbitals and coordination environments. CeO_2-supported Cu SACs promoted CO_2 activation and deep *CO hydrogenation, achieving 70.3% FE at 400 mA cm^{-2}.[86] Besides, Zn SAs anchored on microporous carbon achieved a high CH_4 FE of 85% at −1.8 V vs SCE, with Zn firmly bound with the O atom of *OCHO, effectively suppressing CO generation.[87]

Multicarbon (C_{2+}) products such as C_2H_4, C_2H_5OH, and CH_3COOH are highly desirable for their energy densities but face selectivity challenges due to competing reaction pathways and complex C−C coupling mechanisms (for example, the competition between the C_{2+} alcohol pathway and the C_2H_4 pathway).[88] Cu-based catalysts remain central to these processes due to favorable adsorption properties for intermediates such as *CO and *H.[89−92] Crystal facet engineering reveals Cu(100) facets preferring ethylene production, while Cu(110) facets promote oxygenates formation.[88] The Cu(100)/(111) facets enabled selective propylene electrosynthesis.[93] Heterointerface engineering like Cu−Pr interfaces strengthened *CO binding, achieving 73% FE for C_{2+} alcohols at 700 mA cm^{-2}.[88] Surface modifications, such as hydrophobic Cu dendrites with stabilized $Cu^{\delta+}$ states, achieved 90.6% C_{2+} FE at a 453.3 mA cm^{-2},[94] while Gd or hexagonal boron nitride (h-BN) integration into Cu_2O preserved Cu^+ sites to enhance yields.[95,96] Alkaline ionic liquid (AIL) concentrated CO_2 on Cu surfaces to deliver 71.6% C_{2+} FE at industrial-scale current density (1.8 A cm^{-2}).[97] Polymeric ionic liquid (PIL) adlayers on Cu surface further suppressed H^+ diffusion, enriching K^+ to facilitate C−C coupling, yielding 82.2% FE at 1.0 A cm^{-2}.[98]

3.2.2. NO_x Reduction into Ammonia. Mitigating hazardous NO_x species is critical to mitigate environmental threats, such as acid rain. While traditional methods reduce NO_x to N_2 by selective catalytic reaction (SCR) using costly reductants like NH_3 and H_2, electrochemical conversion of NO_x to NH_3 offers a dual-purpose strategy. NH_3 serves as both a carbon-free fuel and a precursor for fertilizers and pharmaceuticals.[22] The conventional Haber-Bosch Process (HBP) for NH_3 synthesis faces challenges including energy intensity, fossil fuel consumption, and CO_2 emissions. Electrochemical NH_3 synthesis via NO reduction is promising due to NO's high activity as a nitrogen source and its favorable thermodynamic reduction potential (∼0.71 V vs RHE), enabling high NH_3 yields and FE.[22]

Despite atmospheric NO concentrations typically <5%, most NO reduction reaction (NORR) studies focus on high-purity or concentrated NO streams,[99−101] highlighting the need for catalysts under dilute conditions. Although Cu is a potent catalyst for pure NO reduction, it showed a limited FE of 8.20% for 1% NO-to-NH_3 conversion.[99] In contrast, low-coordination Ru nanosheets performed excellently in dilute NO environments (1%), delivering 65.96% NH_4^+ FE and a robust NH_3 production rate (45.02 μmol h^{-1} mg^{-1}).[99] This exceptional performance at dilute NO levels highlights the potential of Ru-based catalysts for practical electrochemical NORR.

The limited solubility of NO in water (∼1.94 mM at 25 °C) constrains NH_3 production at low concentrations due to mass transfer limits.[102] Metal-based coordination salts, such as EDTA-chelated ferrous ions (Fe^{2+}), have been studied to enhance the NO absorption. This approach leverages the Brown-ring reaction mechanism, where Fe^{2+} coordinates with NO to improve solubility.[103] A neutral-pH phosphate buffer solution (PBS) containing an EDTA-Fe^{2+} metal complex (EFeMC) was employed to control NO solubility, with higher EFeMC concentration (50−200 mM) boosting current density (∼34 mA cm^{-2}).[104] To mitigate the impact of EDTA on NH_3 detection, ferrous citrate (Fe^{II}Cit) was utilized as the

https://doi.org/10.1021/acs.est.5c06634
Environ. Sci. Technol. 2025, 59, 24177−24196

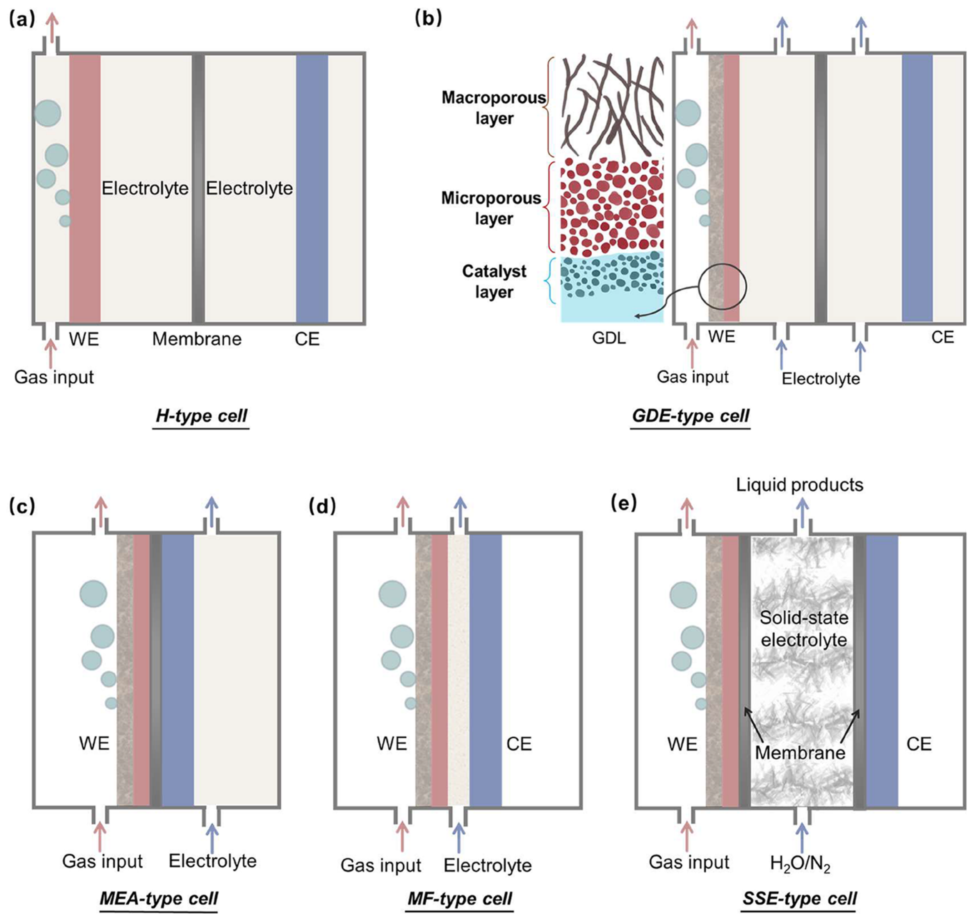

Figure 4. Schematic representation of different reactor configurations: (a) H-type cell; (b) GDE-type cell; (c) MEA-type cell; (d) MF-type cell; and (e) SSE-type cell.

electrolyte, achieving a NH_3 yield of 14.6 μmol h^{-1} cm^{-2} and 65.2% FE using Au/rGO electrodes.[105]

TMO catalysts display outstanding performance in NORR. Specifically, Cu-based catalysts display superior selectivity for NH_3 over H_2.[101] At a potential of −0.9 V vs RHE, a Cu foam electrode achieved an NH_3 synthesis rate of 517.1 μmol h^{-1} cm^{-2} with 93.5% FE and 100-h stability. Modifications such as g-C_3N_4 decoration or integration with porous TiO_2 (Cu/P-TiO_2) further enhance catalytic activity by improving electronic properties or NO adsorption.[106,107] Pressurized electrolysis with a Cu nanowire array monolithic electrode elevated the NH_3 production rate to 10.5 mmol h^{-1} cm^{-2} with 96.1% FE at 1000 mA cm^{-2}.[108] Additionally, hexagonal Co nanosheets and NiNC@CF electrocatalysts achieved an impressive NH_3 yield owing to the unique electron structures and proton shuttle effect or robust substrate-catalyst interaction,[109,110] while P-doped MoS_2 nanospheres displayed a maximal NH_3 FE of 69% and 388.3 μg h^{-1} $mg_{cat.}^{-1}$ yield, with P dopants assisting the activation and hydrogenation of NO.[111]

SACs have gained attention in NORR relating to the coordination environment around the metal center.[22,112,113] SACs incorporating Al, Mn, Fe, Cu, and Nb on B,N codoped carbon nanotubes exhibited high NH_3 yield, with Nb-SACs nearing the US Department of Energy (DOE) target.[113] A W-SAC with $W_1{-}O_5$ motifs on MoO_{3-x} nanosheets achieved 91.2% FE and 308.6 μmol h^{-1} cm^{-2} NH_3 yield by facilitating NO activation and promoting H_2O dissociation while suppressing *H dimerization.[114]

3.3. Synergistic Control of Air Pollutants and GHGs.

Air pollutants and GHGs are often coemitted during fossil fuel combustion, highlighting the importance of integrated control strategies to reduce costs while addressing climate change and environmental degradation. Key industrial sectors, such as coal-burning power plants, steel production, and cement manufacturing, are major sources of SO_2 and NO_x, as well as CO_2. Technological advancements can promote the synergistic control of carbon, sulfur, and nitrogen oxides.[5] The energy, industrial processes, and product use and waste sectors are the primary sources of CH_4 and N_2O emissions. For instance, wastewater treatment plants (WWTPs) represent a significant source of greenhouse gas emissions in China, accounting for 8.7% of CH_4 and 22.1% of N_2O emissions in 2022.[115] This highlights the potential for synergistic treatment strategies to achieve both environmental and economic benefits. While electrocatalytic N_2O reduction currently focuses on pollutant degradation (yielding low-value N_2),[116,117] alternative pathways for N_2O resource utilization leverage its role as a weak oxidant. For example, N_2O can enable the covalorization of CH_4 and N_2O through syngas production, offering a more sustainable approach to emission mitigation.[118]

Electrochemical processes offer a promising approach for the simultaneous treatment of complex air pollutants with high technological and economic efficiency. For example, the coreduction of NO and CO_2 can facilitate urea synthesis, where critical intermediates (*CO and *NH_2) form a C−N bond in a cascade reaction on Zn nanobelts, achieving a urea

https://doi.org/10.1021/acs.est.5c06634
Environ. Sci. Technol. 2025, 59, 24177−24196

yield of 15.13 μmol h^{-1} mg^{-1}.[119] This strategy not only supports carbon-neutral goals but also promotes a sustainable nitrogen cycle. To date, nitrate has served as the predominant nitrogen feedstock for electrocatalytic urea synthesis via CO_2 coreduction. Research employing NO as an alternative nitrogen source constitutes a nascent field requiring significant further development. Additionally, integrating CH_4OR with CO_2RR enabled methyl formate production at 1660 μmol h^{-1} cm^{-2} with ∼15.2% EE.[10] In this system, CH_4 was first converted into CH_3Cl using an IrO_2 nanowire anode, followed by nucleophilic attack by $HCOO^-$ derived from CO_2 to produce methyl formate. This integrated approach exhibited excellent stability at industrial-level current densities (700 mA cm^{-2}) and a 3-fold improvement in yield and EE compared to those of separate processes, showing an efficient strategy of utilizing GHGs.

Electrochemical reduction systems have demonstrated effectiveness in CO_2RR and NO_x removal even in SO_2-containing flue gas.[120,121] For instance, in a simulated flue gas mixture (15.0% CO_2, 3.6% O_2, 0.3% SO_2, and 81.1% N_2), a β-Bi_2O_3-derived bismuth catalyst maintained nearly identical $HCOO^-$ current densities and FE as in pure CO_2, demonstrating industrial applicability.[121] Another system employed Fe(II)(EDTA) to absorb and electrochemically convert NO_x to N_2 while regenerating Fe(II)(EDTA).[120] With activated carbon catalysis and $NaSO_3$ assistance, 99% of NO_x and 98% of SO_2 removal were achieved at low energy consumption.[103] Alternative strategies include the simultaneous electrochemical oxidation of NO and SO_2 to HNO_3 and H_2SO_4. In an Ag(II)/Ag(I)-based mediated system, simulated flue gas (100−400 ppm NO and SO_2) achieved near-complete removal, with SO_2 enhancing NO oxidation efficiency.[122,123] Additionally, integrated electrochemical cells can co-remove NO and CH_4 effectively, further illustrating the versatility of electrochemical approaches for multipollutant control.[124]

4. REACTOR DESIGN

Recent advances in electrocatalyst development have been complemented by a growing recognition of the critical role of reactor design and operating conditions in determining electrochemical performance. Electrochemical reactor systems can be optimized through two perspectives: internal configuration and external field integration, as detailed below.

4.1. Reactor Configuration.

Batch reactors, such as the widely used H-type cell, are common in laboratories due to their easy assembly, simple operation, and cost-effectiveness.[125] However, their performance is often limited by low gas solubility in liquid electrolytes, resulting in low current densities and low FE. To overcome this limitation, advanced reactor designs with reduced resistance and enhanced mass transfer efficiency have been developed,[126] including gas diffusion electrode (GDE)-type, membrane electrode assembly (MEA)-type, microfluidic (MF)-type, and solid-state electrolyte (SSE)-type cells (Figure 4).

4.1.1. Gas Diffusion Electrode (GDE)-Type.

While flow cells improve the mass transfer compared to conventional H-type cells, they still suffer from low gas solubility. GDE-type cells overcome this limitation by creating an efficient three-phase interface that reduces gas diffusion pathways, from ∼50 μm (in an H-cell) to ∼50 nm (in a GDE-type cell).[127] This architecture combines a macroporous GDL for efficient reactant transport with a microporous hydrophobic polytetrafluoroethylene (PTFE) to separate the electrolyte from the gaseous stream while maintaining essential electric contact (Figure 4b).

Such designs have enabled remarkable performance enhancements, enabling high-rate CO_2 electrolysis at current densities over 200 mA cm^{-2}, while the H-cell suffers from a limiting current density of the order of 10 mA cm^{-2}.[128] A 7-fold increase in CO partial current density was obtained with a nearly 90.0% FE_{CO} at 450.0 mA cm^{-2} using a GDE-type cell[129] and further increase to 3.2 A cm^{-2} for CO_2RR was obtained by enhancing the hydrophobicity of catalysts.[130] An enhanced gas reactant concentration at the gas-liquid-solid interface can be achieved by efficient wettability modification or optimized electrode structure design, such as bioinspired artificial lung-type Au/PE catalyst system.[131,132] The remarkable mass transport characteristics of GDEs make them particularly effective for processing dilute gaseous reactants. For example, by integrating nanoscale zerovalent iron into CB GDE, a 96% FE for NH_3 production using feed gas with only 1% NO was obtained.[133] However, the influence of the GDE architecture on reaction pathways requires careful consideration to fully optimize system performance.

Material selection plays a critical role in the GDE performance, particularly for oxidation reactions. Conductive oxides, such as TiO_2/RuO_2, when pressed and sintered with PTFE particles, demonstrate superior stability compared to conventional CB graphite, especially under high positive potentials.[134] This material advantage is exemplified in the electrosynthesis of CH_3OH from CH_4, where the incorporation of 5.6% V_2O_5 into TiO_2/RuO_2/PTFE composites increased the current efficiency from 30% to 57%.[134,135]

However, GDE-type cells face operational challenges that require engineering solutions. The issue of electrode flooding, caused by gradual loss of hydrophobicity or pressure imbalances, can be mitigated through optimized flow rate control, hydrophobic additives, or novel binder-free electrode designs.[136−138] Additionally, conventional carbon-supported electrodes face critical stability challenges under high-current operation, including carbon support degradation and insufficient catalyst-substrate adhesion. These limitations highlight the need for robust alternatives. The self-standing and binder-free GDEs emerged as promising solutions, demonstrating both exceptional electroactive species retention and superior mass transfer performance at industry-relevant current densities.[139,140]

4.1.2. Membrane Electrode Assembly (MEA)-Type.

The conventional flow cell design, while effective in separating the anode and cathode chambers through ionic exchange membranes (IEMs), suffers from significant charge carrier resistance. The MEA-type cell addresses this limitation through a zero-gap configuration, where catalyst layers are directly pressed onto both sides of the IEM (Figure 4c). This design greatly reduces the ohmic resistance, leading to an improved EE. MEA systems can operate in two ways: fully vapor-fed or with liquid electrolyte on one or both sides, offering precise control over pH and the catalyst microenvironment while minimizing GDL flooding through reduced liquid electrolyte contact.[141]

The MEA configuration enables several key advantages, including the use of humidified gaseous reactants instead of liquid electrolytes, which facilitates internal CO_2 recapture and recycling, eliminating the need for downstream separation.[84] Moreover, it resolves the trade-off between the FE and current density. For example, when employing humidified CO_2 feed,

https://doi.org/10.1021/acs.est.5c06634
Environ. Sci. Technol. 2025, 59, 24177−24196

CO_2RR could reach high selectivity (>95% FE_{CO}) at high current densities up to 150 mA cm^{-2}.[142] As the humidified gaseous CO_2 flow rates increased from 2 to 100 SCCM, the selectivity toward CO increased from 90 % to 99%.

Vapor-fed MEA systems offer benefits for product collection and separation.[143] For example, methanol (boiling point of 65 °C) can be selectively evaporated from aqueous electrolytes (at ∼80 °C), preventing complete oxidation.[143] This approach also overcomes the challenges associated with decreasing methane solubility at elevated temperatures. Various catalysts, including metal oxides supported on SnO_2 with a ceramic proton conductor such as $Sn_{0.9}In_{0.1}P_2O_7$, have demonstrated excellent performance in CH_4 oxidation in a MEA cell at 100 °C, with V_2O_5 achieving 88.4% CH_3OH selectivity and 61.4% current efficiency.[144]

MEA represents the most practical solution for achieving industrial-scale current densities while maintaining high EE and product selectivity.[145] For example, $Sb_{0.1}Sn_{0.9}O_2$ electrocatalysts in a MEA cell delivered 200 h stability with 82% $FE_{formate}$ at 500 mA cm^{-2}, achieving 39.1% full-cell EE and a $HCOO^-$ formation production rate of 8.0 mmol h^{-1} cm^{-2}.[146] With optimized hydrophobic coatings, MEA achieved exceptional stability over 500 h at 200 mA cm^{-2} while maintaining FE_{CO} of over 90%.[145]

Although MEA applications in the electrochemical conversion of NO to NH_3 remain underexplored, their adoption in catalyst evaluations could provide more reliable performance results compared to the H-type cell.[147] While MEA configurations are currently the most promising CO_2RR design for industrial scale-up, several critical challenges must be addressed for successful implementation.[148] Beyond mitigating membrane degradation, selecting robust membranes that combine high ionic conductivity with exceptional durability is crucial for enabling prolonged operation in scalable systems and reducing operational expenses.[149] For large-scale development, two parallel development pathways are essential: (1) optimizing large-area electrolyzers to simultaneously minimize ohmic resistance and enhance operational stability,[149] and (2) addressing stack integration challenges through the development of low-resistance large-sized electrode catalysts and engineered flow channels to ensure homogeneous electrolyte distribution across extended electrode surfaces.[150] Furthermore, the unique configuration of MEA systems necessitates sophisticated water management strategies to prevent performance-limiting water deficiency, particularly at high-current-density operation, since water molecules must permeate from the anolyte to serve as the exclusive proton source for CO_2RR.[151]

4.1.3. Microfluidic (MF)-Type. While membrane-based systems face challenges including high cost, reduced ion transport efficiency, and membrane degradation during operation, MF-type cells offer a promising membrane-free alternative.[152] The MF cell consists of three parts: anode chamber, cathode chamber, and ultrathin electrolyte chamber (<1 mm) to reduce osmotic pressure on GDL and control the intersection of reactants and products under laminar flow conditions (Figure 4d). This configuration allows continuous flow operation and individual electrode analysis, making it an ideal electrochemical analysis tool.[153]

Electrolyte conditions are crucial in an MF cell. Initial investigation using Sn catalysts for CO_2RR revealed that acidic conditions (pH = 4) enhanced both current densities and formic acid selectivity compared to neutral or alkaline environments.[154] Advanced pH differential systems demonstrated even greater improvements, with a dual-electrolyte system (catholyte pH = 2, anolyte pH = 14 separated by a 0.01 cm-thick polyvinyl chloride sheet) achieving triple the reactivity and boosting FE from 81.6% to 95.6% compared to a single neutral electrolyte configuration.[153] Electrolyte composition studies in CO_2RR further identified concentration effects and anion-specific impacts (OH^-, HCO_3^-, and Cl^-) on reaction onset potentials.[155] Additional critical parameters requiring optimization include the gas concentration, flow rate, channel length, GDE structure, and overall cell architecture.

MF cells exhibit superior operational stability compared to MEA by eliminating membrane-related charge transfer issues. This advantage is exemplified in CO_2RR using cobalt phthalocyanine (CoPc) catalyst: while the MEA configuration showed a rapid FE_{CO} decline from 95 % to 60% within 5 h, the MF cell maintained >80% FE_{CO} over 100 h at 50 mA cm^{-2}.[142] This performance difference was attributed to proton depletion at catalyst-membrane interfaces in MEAs rather than catalyst degradation.

However, the absence of physical electrode separation in MF cells introduces some limitations. Products generated at each electrode experience opposing electromagnetic forces, leading to undesirable reoxidation or secondary reduction that compromises both FE and EE. This fundamental constraint currently limits the practical application of MF systems despite their other advantages.

4.1.4. Solid-State Electrolyte (SSE)-Type. To enhance the efficiency of liquid product generation and minimize the need for postproduct separation, SSE-type electrolyzers have emerged as an innovative solution. Unlike conventional flow cells that rely on liquid electrolytes, SSE cells utilize functionalized porous solid electrolytes as ion transport channels, with AEM and CEM positioned on either side (Figure 4f). This design was first employed in CO_2RR in 2019, enabling the direct production of electrolyte-free HCOOH.[156] The system operated with humidified CO_2 fed to a cathodic GDE completely avoiding liquid electrolytes, while the anode was circulated with H_2SO_4 solution. The porous polymer electrolyte, incorporating sulfonic acid functional groups for H^+ conduction and quaternary amino functional groups for $HCOO^-$ conduction, allowed continuous extraction of the pure HCOOH product through a deionized water stream. Bi catalyst demonstrated stable production of 0.1 M HCOOH for 100 h.

Further advancements led to the development of an entirely liquid-free, all-solid-state reactor designed to enhance both product concentration and generation rates.[157] In this system, CO_2 was reduced to formic acid vapor, which was carried by N_2 flow through the SSE, while H_2 gas replaced liquid acid at the anode to supply protons. This innovative approach resulted in a high-activity ($HCOO^-$ partial current densities >440 mA cm^{-2}), high-selectivity (>97% FE), high-stability (100 h), and the production of highly concentrated pure formic acid solutions.

The versatility of SSE-cells has been demonstrated with various catalyst systems, including Bi_3S_2-ascorbic acid hybrid catalyst (BS/VC)[74] and single-atom Pb-alloyed Cu catalyst (Pb_1Cu),[158] both achieving continuous industrial-scale formic acid production for 100 or 180 h. Notably, SSE electrolyzers have also been adapted for C_2H_5OH synthesis, with a Cu catalyst producing 90% pure C_2H_5OH solutions at 600 mA over 50 h.[94] While SSE cells show great promise for diverse

https://doi.org/10.1021/acs.est.5c06634
Environ. Sci. Technol. 2025, 59, 24177−24196

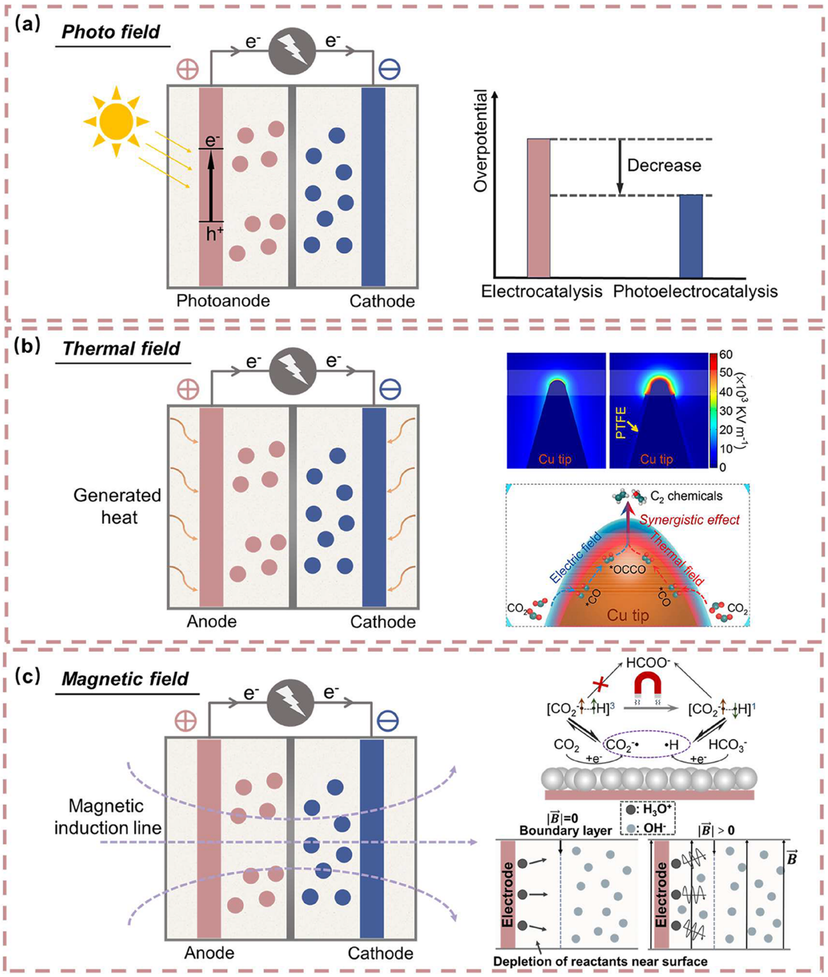

Figure 5. Schematic representation and mechanism of electrocatalytic system with external field: (a) photo field, (b) thermal field (reproduced with permission from ref 174; Copyright 2022 American Chemical Society), and (c) magnetic field (reproduced with permission from refs 181 and 184; Copyright 2020 American Chemical Society; Copyright 2022 Elsevier).

liquid product generation, several critical challenges must be addressed for practical implementation. First, the development of defect-free, mechanically robust IEMs on an industrial scale remains a fundamental challenge. Second, during device scale-up, the precise control of the SSE layer morphology becomes essential. Specifically, minimizing variations in particle packing density and reducing interparticle gaps are important to ensure uniform SSE/membrane interfacial contact and to enhance ionic conductivity throughout the entire active area. Third, rational liquid flow management systems should be implemented to simultaneously achieve efficient product collection, effective gas bubble removal, full utilization of the electroactive area, and minimized pressure drops across the SSE layer.[159] These interconnected engineering considerations will be crucial for transitioning SSE technology from lab-scale demonstrations to commercially viable systems.

4.2. Coupling with External Fields. Incorporating external fields alongside electric fields is emerging as a promising way to enhance the activity or selectivity of gas-involved electrocatalysis. Specifically, photo, thermal, and magnetic fields (Figure 5) have shown great potential in enhancing reaction kinetics and thermodynamics by facilitating charge and mass transfer. The integration of such external fields provides a versatile means of engineering electrochemical processes, enabling convenient, continuous, reversible, dynamic, and universally applicable control mechanisms.[160]

4.2.1. Photo Field. Photoelectrochemical (PEC) systems combine the advantages of electrocatalytic and photocatalytic processes. In these systems, light absorption by a photoanode excites electrons to the conduction band, which are then transferred to the cathode via an external circuit (Figure 5a). An external bias or tandem cell configurations enable efficient separation of photogenerated electron-hole pairs,[8] enhancing anodic oxidation efficiency and charge transfer across the cell. This photo field application can further decrease the reaction overpotential compared to conventional electrocatalysis. For instance, the WO_3-OV photoanode achieved a high CH_3Cl FE of 57.2% at only 0.9 V vs RHE, while the $CoNi_2O_x$ electrocatalyst required substantially higher potentials (>1.6 V vs RHE) for CH_3Cl production.[14,161] PEC systems offer several benefits, including controllable selectivity and reaction rates by applied potential, adjustable electrode properties with the cocatalyst, a wide range of compatible catalysts, and adaptable device designs.[162,163]

Mechanisms for CH_4, CO_2, and NO_x treatment vary in the PEC systems. At the photoanode, photogenerated holes directly oxidize gaseous reactants or facilitate water oxidation (with water vapor), producing ROS such as •OH, which mediate anodic oxidation. In an ideal PEC CH_4OR system,

https://doi.org/10.1021/acs.est.5c06634
Environ. Sci. Technol. 2025, 59, 24177−24196

ROS lowers the energy barrier for C−H bond activation, promoting CH_4 dehydrogenation, while electrons are transferred to the cathode, producing H_2. For NO treatment, oxidation dominates the process, rather than reduction to NH_3. During this process, ·OH radicals drive complete NO oxidation, while photogenerated electrons suppress O_2 activation at the counter electrode, preventing partial NO oxidation via $\cdot O_2^-$ formation.[164] In contrast, the PEC CO_2RR system relies on a dark cathode receiving photogenerated electrons to initiate CO_2RR, while the photoanode governs light absorption and electron-hole pair generation.[165] Enhanced light-harvesting capabilities directly correlate with higher photoconversion efficiency.

Intermediate control is critical for efficient PEC processes, especially in C−C coupling for multicarbon compounds. For instance, NiO-polyoxometalate (POM) subnanocoils stabilized the *COOH intermediates via electron delocalization in POM clusters, achieving 4.48 mmol g_{cat}^{-1} h^{-1} productivity and >99% selectivity for CH_4-to-C_2 conversion.[166] Similarly, a graphene/silicon carbon composite catalyst facilitated electron transfer from SiC to active sites, stabilizing intermediates to yield 17.1 mmol g_{cat}^{-1} h^{-1} ethanol from CO_2 with >99% selectivity.[167]

Nitrate accumulation during PEC NO treatment typically occupies reaction sites, reducing the long-term reactivity. Ni-modified NH_2-UiO-66(Zr) on nickel foam addressed this issue by enabling selective NO removal and nitrate storage simultaneously.[164] By tuning external bias to optimize ·OH generation, 82% NO elimination was achieved at 0.3 V without NO_2 byproducts. The photoanode's 3D porous morphology enhanced nitrate diffusion and storage, maintaining system stability and selectivity.

Dual-function PEC systems enable simultaneous anodic and cathodic gas treatment. For example, a single PEC system achieved concurrent SO_2 desulfurization and H_2O_2 generation, boosting photocurrent by 40% and achieving H_2O_2 evolution of 58.8 μmol L^{-1} h^{-1} cm^{-2}, which was 5-fold higher than SO_2-free conditions.[168] PEC systems also show potential for treating mixed acid gases (NO_x and SO_2).[169] NaOH pretreated waste gas underwent photoanodic SO_2 conversion to $SO_4^{\bullet-}$ and cathodic NO_x^- reduction to NH_4^+. As a result, $SO_4^{\bullet-}$-NH_4^+ reactions selectively oxidized NH_4^+ to N_2 while reducing $SO_4^{\bullet-}$ to SO_4^{2-} with 99.9% TN removal and 100% SO_3^{2-} conversion.

Gas-phase reactant challenges arise from limited charge transport in ambient air.[170] CNTs in TiO_2-based photoanodes bridged electron transfer between TiO_2 and stainless-steel meshes, enhancing hole exposure to flowing NO. Afterward, a more effective TiO_2/fluorine-doped tin oxide (FTO) photoanode achieved efficient indoor NO removal at low bias voltages via rapid photoelectron-hole separation.[171]

4.2.2. Thermal Field. Temperature plays a crucial role in electrochemical reactions by affecting charge transfer at electrolyte-electrode interfaces, diffusion kinetics, electric double-layer formation, and overall electrode reactivity.[160,172] Therefore, thermal fields can enhance reaction rates by facilitating kinetic processes,[173] making their integration into electrochemical systems a promising strategy for improving reactivity and selectivity. Thermal-assisted electrocatalysis involves techniques such as thermo-electrocatalysis and electrical-, light-, or magnetic-induced heat generation.[160]

In the CO_2RR, increasing the applied potential or bulk electrolyte heating is a simple way to intensify both the electric and thermal fields. However, this approach can also lead to an increase in the HER and favors C_1 product generation. A more efficient strategy involves localized electric-thermal field enhancement (Figure 5b). For example, coating Cu nanoneedle (Cu NN) tips with PTFE amplified the electric and thermal fields by ∼3-fold with increasing PTFE coverage.[174] The enhanced electric field lowered the Gibbs free energy (ΔG) of C−C coupling, and the stronger thermal field accelerated the C−C coupling reaction rate. The boosted adsorption and dimerization of *CO intermediates facilitated the selectivity for C_2 products, achieving over 86% FE_{C2} at a partial current density of >250 m Acm^{-2} with a record-high C_2 TOF of 11.5 ± 0.3 s^{-1} Cu $site^{-1}$.[175]

A similar tip-induced thermal field was also observed in a high-curvature Bibased catalyst with an amorphous layer (HS2-Bi).[172] Under a 1000 mA current, the catalyst's temperature rose by ∼63.0 K. While elevated temperatures generally favor H_2 generation over $HCOO^-$ production, HS2-Bi's high curvature structure localized the electric field, selectively suppressing H_2 and maintaining $HCOO^-$ output. This study demonstrated how self-generated local electrothermal fields can simultaneously enhance the reaction kinetics and tune selectivity.

4.2.3. Magnetic Field. Magnetic fields have recently emerged as a promising, noncontact, and environmentally friendly approach to enhance electrocatalytic performance.[176,177] By modifying spin structures, facilitating bubble removal through convection, increasing catalytic activity through magnetohydrodynamic effects, and accelerating mass transfer by the Kelvin force effect, magnetic fields can significantly improve reaction kinetics, product yields, and energy efficiency in electrochemical processes.[176−178] The potential reaction mechanisms involved in promoting the CO_2RR with a magnetic field are discussed below as a representative example.

Magnetic fields can promote the CO_2RR by regulating the spin states of radical pairs (Figure 5c). The reaction involves the formation of radical pairs $[CO_2^{-\bullet}\cdots H^\bullet]$, which exist in singlet ($^1[CO_2^{-\bullet}\uparrow\cdots H^\bullet\downarrow]$) and triplet ($^3[CO_2^{-\bullet}\uparrow\cdots H^\bullet\uparrow]$) configurations at a 1:3 ratio.[179] While singlet radical pairs readily form $*HCOO^-$, triplet pairs are spin-forbidden from combining due to the Pauli exclusion principle.[180] An external magnetic field facilitates triplet-to-singlet spin conversion, thus increasing the amount of reactive singlet radical pairs to enhance CO_2RR efficiency.[181] Experimental results demonstrated a dramatic increase in electrocatalytic current under a magnetic field, with the effect amplified at higher $KHCO_3$ concentrations and more negative electrode potentials. The yield of formic acid doubled under a 0.9 T magnetic field compared to magnetic-free conditions.

Magnetic field can also alter the selectivity toward C_1/C_2 products by modifying C−C Coupling dynamics. While C_2 hydrocarbons form through CO dimerization, magnetic fields can lower the activation barrier for this process.[182] For instance, on oxide-derived Cu catalyst, spin-antiparallel electron alignment at asymmetric Cu*−Cu sites promoted C−C coupling, reducing the optimal bias by ∼0.2 V and increasing C_2 FE. However, surface spin polarization can alter *OCHO/*COOH binding energies, suppressing singlet C−C coupling and favoring the formation of C_1 products.[183] This effect was demonstrated on CuO catalysts, where magnetic field application significantly increased the C_1 FE while simultaneously boosting current density and reducing overpotential.

https://doi.org/10.1021/acs.est.5c06634
Environ. Sci. Technol. 2025, 59, 24177−24196

Magnetic fields improve mass transport (Figure 5c) and reduce energy consumption in the CO_2RR systems. The Lorentz force induces convective fluid motion, enhancing ion transport both in bulk solution and near electrode surfaces.[184] In one configuration, a perpendicular neodymium iron boron (NdFeB) magnet generated fluid convection that reduced local pH gradients, increasing the current density and selectivity while lowering energy consumption by 15% in a GDE flow cell. Similarly, NiFe-based bimetallic anodes under magnetic fields exhibited reduced overpotentials.[185] The magnetohydrodynamic effect further enhanced the mass transfer, achieving 7−64% energy savings compared to that of IrO_2 anodes without a magnetic field at CO partial current densities over 300 mA cm^{-2}.

5. CHALLENGES AND PERSPECTIVES

The sustainable mitigation of industrial air pollutants and GHGs has become a global priority. Electrocatalysis has emerged as a promising technology for converting these gases due to its possibility to operate under mild conditions, compatibility with renewable energy sources, adjustable reaction pathways for selective product formation, and relatively simple infrastructure requirements. While recent laboratory-scale research has demonstrated progress, key challenges, including limited mass transfer efficiency and complex process control, hinder the industrial scalability of gas-phase electrochemical systems.

5.1. Regulation of Each Involved Gas Component. The regulation of individual gas component in electrocatalytic systems requires the comprehensive optimization of catalyst properties. Achieving industrial-level current densities necessitates careful design of electrocatalysts, where activity and selectivity are fundamentally governed by structural characteristics, surface chemistry, and electronic properties.[186] Recent advances have demonstrated that strategic modifications through alloying, structural and surface designing, interface and strain engineering can significantly enhance performance.[187] Certain 2D nanomaterials exhibit unique electronic states (e.g., increased density of states near the Fermi level and altered band-edge potentials and band gap) and physicochemical properties (e.g., enhanced electrical conductivity and carrier mobility) that make them catalytically active.[186,188] Lattice strain and surface defects are known to increase active site exposure while simultaneously tailoring local chemical environments and electronic states of materials.[189−191] These unsaturated sites can directly interact with reactants or intermediates as active centers, enhancing electrocatalytic activity.[192] Additionally, the integration of machine learning and computational screening has emerged as a powerful tool for identifying active electrocatalyst structures, enabling rational design based on high-quality in situ characterization data and theoretical simulations of intermediate interactions.[193,194]

Beyond intrinsic electrocatalyst properties, practical implementation demands innovative solutions to overcome mass transfer limitations in gas-phase electrocatalysis.[130] Transforming from conventional H-cell configurations into advanced configurations, such as GDE-type, MEA-type, MF-type, and SSE-type cells, has improved the gas accessibility to active sites. Strategic electrolyte engineering, including the use of coordinating species like Fe^{2+}-EDTA complexes for NO adsorption or tailed salt solutions for organic compound adsorption, provides an effective pathway to enhance reactant concentration at the electrode interface. Equally important is the precise control of three-phase boundary properties through wettability modification, which ensures a stable gas supply even at elevated current densities.[131] These interfacial engineering approaches must be integrated with optimized fluid dynamics, where novel flow channel architectures inspired by spiral, corrugated, and biological patterns have demonstrated remarkable improvements in mass transport characteristics. The growing application of computational fluid dynamics simulations has further accelerated the development of efficient flow field designs tailored to specific reaction requirements.[152]

5.2. Regulation of Complex Reaction Conditions. The electrochemical treatment of industrial waste gases presents significant challenges due to the inherent complexity and variability of gas compositions. A primary concern is the competitive adsorption of multiple pollutant species at catalytic sites, where different components compete on the catalyst surface and follow divergent reaction pathways. This multicomponent interference could be mitigated through the development of cascade reaction systems designed to sequentially process different gas constituents. Another critical issue is the fluctuating nature of industrial emissions, where sudden load changes can cause dramatic variations in pollutant concentrations. Concurrently, overlapping potential windows of competing reactions frequently result in poor product selectivity. The mismatch in reaction kinetics between anodic and cathodic processes creates additional complications, often manifested as imbalances in mass transport and reaction rates that limit system efficiency.

The electrocatalytic system of mixed-gas streams introduces additional challenges in electrolyte management and product separation. Substantial fluctuations in electrolyte composition and pH occur due to competing reactions, which may cause catalyst detachment and carbonate precipitation that blocks active sites, such as electrolyte acidification from H_2SO_4 formation during SO_2RR and localized pH increases from CO_2RR and NORR. Enhancing product concentration is essential to maintain economic viability, as it increases product value while reducing downstream separation energy and costs. Pretreatment steps such as gas enrichment may be required to achieve higher purity. Additionally, optimizing electrolyzer selection and electrocatalyst design can enhance product yield and purity by enhancing conductivity, catalytic activity, and selectivity. For the downstream gas products separation, combining effective separation technologies (e.g., pressure swing adsorption) with strategies to increase single-pass conversion efficiency can lower separation costs.[195] For liquid products, SSE-type reactors offer distinct advantages by enabling in situ product separation, thereby decreasing the energy input of distillation processes. These integrated solutions address both the technical challenges of a mixed-gas electrocatalytic system and the economic requirements for industrial implementation.

5.3. Achieving Practical Implementation. The transition from lab-scale to industrial implementation of electrocatalytic systems requires significant advancements in reactor design and process engineering. Critical improvements in membrane and device architectures are essential to meeting industrial demands. While GDE and MEA-type cells exhibit cross-reaction compatibility (CO_2RR, NORR, CH_4OR), the limited scope of MF-type and SSE-type beyond CO_2RR underscores a critical research gap. Addressing this gap through configuration-specific optimization and reaction pathway

https://doi.org/10.1021/acs.est.5c06634
Environ. Sci. Technol. 2025, 59, 24177−24196

engineering could bridge laboratory innovation to industrial-scale electrochemical manufacturing. For instance, optimizing SSE-type cells may involve thickness control of the SSE layer to reduce ohmic resistance and enhance electron transfer efficiency.[196] Integrating resin wafers into SSE layers can enhance reactor scalability and reproducibility while boosting ionic conductivity via uniform membrane contact and conductive gap-filling binders.[159] Additionally, the integration of external fields in a large-scale application requires a deeper mechanistic understanding and engineering solutions.

Scaling strategies must address both technical and operational challenges. Modular system design offers a flexible approach to handling complex gas mixtures while enabling development in diverse settings, including remote locations powered by renewable energy.[197] The integration of electrocatalytic systems with complementary technologies, such as tandem electro-thermocatalytic processes, could provide comprehensive solutions for CO_2-rich natural gas.[198] To establish the commercial viability of gas covalorization systems, rigorous techno-economic analysis (TEA) and life cycle assessment (LCA) should be conducted using pilot-scale operational data. These comprehensive evaluations should address three fundamental aspects: (1) the techno-economic assessment requires systematic examination of both capital expenditures (CAPEX) and operating expenditures (OPEX), with particular attention to critical performance benchmarks (e.g., minimum 5 year stability for electrolyzer components, single-pass conversion efficiencies of 30% for C_1 and 15% for C_2 products[9]), product purity specifications, and overall system energy efficiency; (2) the environmental impact evaluation requires complete cradle-to-gate life cycle analysis to quantify the carbon footprint and resource utilization efficiency across the entire value chain, accounting for all material inputs and energy flows; (3) the assessment should identify key optimization opportunities by analyzing cost distribution patterns, operational parameters sensitivities, and scale-up effects on system performance. Together, these multidimensional analyses will provide the essential framework for transitioning these promising coelectrolytic systems from laboratory demonstrations to commercially viable industrial implementations, while ensuring both economic competitiveness and environmental sustainability. As the covalorization of multiple gases is an emerging technology, data from lab-scale and especially pilot-scale studies remain scarce. Therefore, key economic considerations should include product yield and purity, catalyst durability, and energy efficiency.

The high-purity production can be achieved by catalyst engineering and process adjustment. Tuning electrocatalysts with a well-defined local coordination environment and electronic structure close to the active sites may help to enhance the FE.[92] For example, tuning the Cu clusters with particle sizes of <2 nm could enhance the CO_2RR selectivity toward ethanol to an industrial relevance.[199] Besides, a reversed GDE design with CO_2 dissolved in the catholyte and a flow field used as a gas collection chamber eliminates the cost associated with additional separation steps.[200] An integrated electrochemical recovery and separation system shows great potential for largely reducing the cost of electrolyte recovery, product separation, and CO_2 capture.[201]

Catalyst stability remains a fundamental challenge, with degradation mechanisms including chemical corrosion, particle agglomeration, phase transformation, and surface poisoning, particularly under extreme pH conditions or high potential operation. Advanced stabilization strategies, ranging from atomic-level site engineering to self-healing materials with dynamically stable interfaces and optimized GDL, are being developed to address these issues. While SAC and in situ product extraction methods show potential for reducing energy demands,[67,143] the intermittent nature of renewable power sources introduces additional system complexity.[202] This issue requires careful consideration of energy storage and power conditioning solutions to ensure stable operation. Further energy input reduction can be achieved through external-field coupling strategies regarding local conditions, in addition to photoelectro, thermo-electro, and magnetic-electro catalysis. Developing piezo-electro catalysis can potentially reduce the activation barrier and dynamically optimize energy allocation with external stress fields.[160,203,204]

The successful integration of these materials and engineering innovations presents a multifaceted approach to addressing the fundamental challenges in gas-involved electrocatalysis. From atomic-scale catalyst design to macroscopic reactor optimization, each advancement contributes to overcoming the limitations that have hindered practical implementation. As the field progresses, the synergy among computational prediction, advanced characterization, and system-level engineering will yield more sophisticated solutions for efficient and selective electrochemical gas conversion. These developments not only advance fundamental understanding but also pave the way for industrial-scale applications of electrocatalytic technologies in gas-involved environmental remediation and energy conversion.

ASSOCIATED CONTENT

Supporting Information

The Supporting Information is available free of charge at https://pubs.acs.org/doi/10.1021/acs.est.5c06634.

Performance metrics of representative catalysts for electrocatalytic utilization of typical air pollutants and GHGs (PDF)

AUTHOR INFORMATION

Corresponding Authors

Le Shi − *State Key Laboratory of Soil Pollution Control and Safety, Key Laboratory of Environment Remediation and Ecological Health, Ministry of Education, Zhejiang Provincial Key Laboratory of Air Pollution Monitoring and Synergistic Control, College of Environmental and Resource Sciences, Zhejiang University, Hangzhou 310058, P.R. China;* orcid.org/0000-0003-1794-1256; Email: le.shi@zju.edu.cn

Zhongbiao Wu − *State Key Laboratory of Soil Pollution Control and Safety, Key Laboratory of Environment Remediation and Ecological Health, Ministry of Education, Zhejiang Provincial Key Laboratory of Air Pollution Monitoring and Synergistic Control, College of Environmental and Resource Sciences, Zhejiang University, Hangzhou 310058, P.R. China;* orcid.org/0000-0003-0182-5971; Email: zbwu@zju.edu.cn

Authors

Liu Huang − *State Key Laboratory of Soil Pollution Control and Safety, Key Laboratory of Environment Remediation and Ecological Health, Ministry of Education, Zhejiang Provincial Key Laboratory of Air Pollution Monitoring and Synergistic*

Control, College of Environmental and Resource Sciences, Zhejiang University, Hangzhou 310058, P.R. China; orcid.org/0000-0003-4364-1812

Ziyan Fu − *State Key Laboratory of Soil Pollution Control and Safety, Key Laboratory of Environment Remediation and Ecological Health, Ministry of Education, Zhejiang Provincial Key Laboratory of Air Pollution Monitoring and Synergistic Control, College of Environmental and Resource Sciences, Zhejiang University, Hangzhou 310058, P.R. China;* orcid.org/0009-0004-6003-4824

Haoyu Yin − *State Key Laboratory of Soil Pollution Control and Safety, Key Laboratory of Environment Remediation and Ecological Health, Ministry of Education, Zhejiang Provincial Key Laboratory of Air Pollution Monitoring and Synergistic Control, College of Environmental and Resource Sciences, Zhejiang University, Hangzhou 310058, P.R. China;* orcid.org/0000-0002-3244-6301

Chuan Xia − *School of Materials and Energy, University of Electronic Science and Technology of China, Chengdu 611731, P.R. China; Yangtze Delta Region Institute (Huzhou), University of Electronic Science and Technology of China, Huzhou 313001, P.R. China;* orcid.org/0000-0003-4526-159X

Shuang Cao − *Department of Environmental Engineering, China Jiliang University, Hangzhou 310018, P.R. China*

Xiaole Weng − *State Key Laboratory of Soil Pollution Control and Safety, Key Laboratory of Environment Remediation and Ecological Health, Ministry of Education, Zhejiang Provincial Key Laboratory of Air Pollution Monitoring and Synergistic Control, College of Environmental and Resource Sciences, Zhejiang University, Hangzhou 310058, P.R. China; ZJU-Hangzhou Global Scientific and Technological Innovation Center, Hangzhou 311200, P.R. China;* orcid.org/0000-0003-2997-571X

Complete contact information is available at: https://pubs.acs.org/10.1021/acs.est.5c06634

Notes

The authors declare no competing financial interest.

ACKNOWLEDGMENTS

This work is supported by Zhejiang Provincial Natural Science Foundation of China (No. LZ24E080004). The authors are grateful to the other group members for the helpful discussion.

REFERENCES

(1) Horowitz, C. A. Paris Agreement. *Int. Leg. Mater.* **2016**, *55* (4), 740−755.

(2) Chen, R.; Zhang, T.; Guo, Y.; Wang, J.; Wei, J.; Yu, Q. Recent advances in simultaneous removal of SO_2 and NO_x from exhaust gases: Removal process, mechanism and kinetics. *Chem. Eng. J.* **2021**, *420*, No. 127588.

(3) De Marco, A.; Proietti, C.; Anav, A.; Ciancarella, L.; D'Elia, I.; Fares, S.; Fornasier, M. F.; Fusaro, L.; Gualtieri, M.; Manes, F.; Marchetto, A.; Mircea, M.; Paoletti, E.; Piersanti, A.; Rogora, M.; Salvati, L.; Salvatori, E.; Screpanti, A.; Vialetto, G.; Vitale, M.; Leonardi, C. Impacts of air pollution on human and ecosystem health, and implications for the National Emission Ceilings Directive: Insights from Italy. *Environ. Int.* **2019**, *125*, 320−333.

(4) Jeffry, L.; Ong, M. Y.; Nomanbhay, S.; Mofijur, M.; Mubashir, M.; Show, P. L. Greenhouse gases utilization: A review. *Fuel* **2021**, *301*, No. 121017.

(5) Li, Z.; Wang, J.; Che, S. Synergistic Effect of Carbon Trading Scheme on Carbon Dioxide and Atmospheric Pollutants. *Sustainability* **2021**, *13* (10), 5403.

(6) Lee, J.; Yang, J.; Moon, J. H. Solar Cell-Powered Electrochemical Methane-to-Methanol Conversion with CuO/CeO_2 Catalysts. *ACS Energy Lett.* **2021**, *6* (3), 893−899.

(7) Kim, K.; Lee, W. H.; Na, J.; Hwang, Y.; Oh, H.-S.; Lee, U. Data-driven pilot optimization for electrochemical CO mass production. *J. Mater. Chem. A* **2020**, *8* (33), 16943−16950.

(8) Dhandole, L. K.; Kim, S. H.; Moon, G.-h. Understanding (photo)electrocatalysis for the conversion of methane to valuable chemicals through partial oxidation processes. *J. Mater. Chem. A* **2022**, *10* (37), 19107−19128.

(9) Shin, H.; Hansen, K. U.; Jiao, F. Techno-economic assessment of low-temperature carbon dioxide electrolysis. *Nat. Sustain.* **2021**, *4* (10), 911−919.

(10) Zhang, Q.; Chen, Y.; Yan, S.; Lv, X.; Yang, C.; Kuang, M.; Zheng, G. Coupling of electrocatalytic CO_2 reduction and CH_4 oxidation for efficient methyl formate electrosynthesis. *Energy Environ. Sci.* **2024**, *17* (6), 2309−2314.

(11) Boyd, M. J.; Latimer, A. A.; Dickens, C. F.; Nielander, A. C.; Hahn, C.; Nørskov, J. K.; Higgins, D. C.; Jaramillo, T. F. Electro-Oxidation of Methane on Platinum under Ambient Conditions. *ACS Catal.* **2019**, *9* (8), 7578−7587.

(12) Deng, J.; Lin, S.-C.; Fuller, J.; Iñiguez, J. A.; Xiang, D.; Yang, D.; Chan, G.; Chen, H. M.; Alexandrova, A. N.; Liu, C. Ambient methane functionalization initiated by electrochemical oxidation of a vanadium (V)-oxo dimer. *Nat. Commun.* **2020**, *11* (1), 3686.

(13) Kim, C.; Min, H.; Kim, J.; Moon, J. H. Boosting electrochemical methane conversion by oxygen evolution reactions on Fe−N−C single atom catalysts. *Energy Environ. Sci.* **2023**, *16* (7), 3158−3165.

(14) Wang, Q.; Li, T.; Yang, C.; Chen, M.; Guan, A.; Yang, L.; Li, S.; Lv, X.; Wang, Y.; Zheng, G. Electrocatalytic Methane Oxidation Greatly Promoted by Chlorine Intermediates. *Angew. Chem., Int. Ed.* **2021**, *60* (32), 17398−17403.

(15) Kim, R. S.; Surendranath, Y. Electrochemical Reoxidation Enables Continuous Methane-to-Methanol Catalysis with Aqueous Pt Salts. *ACS Cent. Sci.* **2019**, *5* (7), 1179−1186.

(16) Yan, L.; Jiang, L.; Qian, C.; Zhou, S. Electrocatalytic conversion of methane: Recent progress and future prospects. *Energy Rev.* **2024**, *3* (2), No. 100065.

(17) Tsai, Y.-F.; Natarajan, T.; Lin, Z.-H.; Tsai, I. K.; Janmanchi, D.; Chan, S. I.; Yu, S. S. F. Voltage-Gated Electrocatalysis of Efficient and Selective Methane Oxidation by Tricopper Clusters under Ambient Conditions. *J. Am. Chem. Soc.* **2022**, *144* (22), 9695−9706.

(18) Kim, J.; Kim, J. H.; Oh, C.; Yun, H.; Lee, E.; Oh, H.-S.; Park, J. H.; Hwang, Y. J. Electro-assisted methane oxidation to formic acid via in-situ cathodically generated H_2O_2 under ambient conditions. *Nat. Commun.* **2023**, *14* (1), 4704.

(19) Huang, B.; He, Y.; Wang, Z.; Zhu, Y.; Zhang, Y.; Cen, K. Ru@Pt/C core-shell catalyst for SO_2 electrocatalytic oxidation in electrochemical Bunsen reaction. *Electrochim. Acta* **2020**, *331*, No. 135315.

(20) Cho, W.-C.; Poo, K.-M.; Mohamed, H. O.; Kim, T.-N.; Kim, Y.-S.; Hwang, M. H.; Jung, D.-W.; Chae, K.-J. Non-selective rapid electro-oxidation of persistent, refractory VOCs in industrial wastewater using a highly catalytic and dimensionally stable IrPd/Ti composite electrode. *Chemosphere* **2018**, *206*, 483−490.

(21) Saha, P.; Amanullah, S.; Dey, A. Selectivity in Electrochemical CO_2 Reduction. *Acc. Chem. Res.* **2022**, *55* (2), 134−144.

(22) Inta, H. R.; Dhanabal, D.; Markandaraj, S. S.; Shanmugam, S. Recent advances in electrocatalytic NO_x reduction into ammonia. *EES Catal.* **2023**, *1* (5), 645−664.

(23) Prajapati, A.; Collins, B. A.; Goodpaster, J. D.; Singh, M. R. Fundamental insight into electrochemical oxidation of methane towards methanol on transition metal oxides. *Proc. Natl. Acad. Sci. U.S.A.* **2021**, *118* (8), No. e2023233118.

(24) Prajapati, A.; Sartape, R.; Kani, N. C.; Gauthier, J. A.; Singh, M. R. Chloride-Promoted High-Rate Ambient Electrooxidation of Methane to Methanol on Patterned Cu−Ti Bimetallic Oxides. *ACS Catal.* **2022**, *12* (22), 14321−14329.
(25) Song, Y.; Zhao, Y.; Nan, G.; Chen, W.; Guo, Z.; Li, S.; Tang, Z.; Wei, W.; Sun, Y. Electrocatalytic oxidation of methane to ethanol via NiO/Ni interface. *Appl. Catal. B: Environ.* **2020**, *270*, No. 118888.
(26) Xie, Z.; Chen, M.; Chen, Y.; Guan, A.; Han, Q.; Zheng, G. Electrocatalytic Methane Oxidation to Ethanol via Rh/ZnO Nanosheets. *Phys. Chem. C* **2021**, *125* (24), 13324−13330.
(27) Ma, M.; Jin, B. J.; Li, P.; Jung, M. S.; Kim, J. I.; Cho, Y.; Kim, S.; Moon, J. H.; Park, J. H. Ultrahigh Electrocatalytic Conversion of Methane at Room Temperature. *Adv. Sci.* **2017**, *4* (12), No. 1700379.
(28) Ma, M.; Oh, C.; Kim, J.; Moon, J. H.; Park, J. H. Electrochemical CH_4 oxidation into acids and ketones on ZrO_2:$NiCO_2O_4$ quasi-solid solution nanowire catalyst. *Appl. Catal. B: Environ.* **2019**, *259*, No. 118095.
(29) O'Reilly, M. E.; Kim, R. S.; Oh, S.; Surendranath, Y. Catalytic Methane Monofunctionalization by an Electrogenerated High-Valent Pd Intermediate. *ACS Cent. Sci.* **2017**, *3* (11), 1174−1179.
(30) Zhang, S.; Huang, B.; He, Y.; Zhu, Y.; Zhang, Y.; Wang, Z. Demetallized PtxNiy/C catalyst for SO_2 electrochemical oxidation in the SI/HyS hydrogen production cycles. *Int. J. Hydrog. Energy* **2021**, *46* (17), 10161−10171.
(31) Dourado, A. H. B.; Silva, N. A., Jr; Neves-Garcia, T.; Braga, A. H.; Rossi, L. M.; Torresi, S. I. C. d. Boosting SO_2 electrocatalytic oxidation reaction on highly dispersed subnanometric Au/TiO_2 catalyst. *Electrochim. Acta* **2022**, *434*, No. 141339.
(32) Huang, B.; He, Y.; Wang, Z.; Zhu, Y.; Zhang, Y.; Cen, K. High-Performance Pt Catalyst with Graphene/Carbon Black as a Hybrid Support for SO_2 Electrocatalytic Oxidation. *Langmuir* **2020**, *36* (1), 20−27.
(33) Safari, F.; Dincer, I. A review and comparative evaluation of thermochemical water splitting cycles for hydrogen production. *Energy Convers. Manage.* **2020**, *205*, No. 112182.
(34) Huang, B.; He, Y.; Zhu, Y.; Wang, Z.; Cen, K. SO_2 Electrocatalytic Oxidation Properties of Pt−Ru/C Bimetallic Catalysts with Different Nanostructures. *Langmuir* **2020**, *36* (12), 3111−3118.
(35) Fouzai, I.; Radaoui, M.; Díaz-Abad, S.; Rodrigo, M. A.; Lobato, J. Electrospray Deposition of Catalyst Layers with Ultralow Pt Loading for Cost-Effective H2 Production by SO_2 Electrolysis. *ACS Appl. Energy Mater.* **2022**, *5* (2), 2138−2149.
(36) Meekins, B. H.; Thompson, A. B.; Gopal, V.; Mehrabadi, B. A. T.; Elvington, M. C.; Ganesan, P.; Newhouse-Illige, T. A.; Shepard, A. W.; Scipioni, L. E.; Greer, J. A.; Weiss, J. C.; Weidner, J. W.; Colón-Mercado, H. R. In-situ and ex-situ comparison of the electrochemical oxidation of SO_2 on carbon supported Pt and Au catalysts. *Int. J. Hydrog. Energy* **2020**, *45* (3), 1940−1947.
(37) Guo, J.-H.; Wei, X.; Sun, W.-Y. A MOF-74(Ni) derived partially oxidized Ni@C catalyst for SO_2 electro-oxidation integrated with solar driven hydrogen evolution. *Sustainable Energy Fuels* **2021**, *5* (14), 3588−3592.
(38) Ying, Z.; Yang, J.; Zheng, X.; Dou, B.; Cui, G. Boosting SO_2-depolarized electrolysis with anodic HI for efficient and energy-saving hydrogen production. *J. Power Sources* **2021**, *491*, No. 229589.
(39) Wu, Z.; Zhang, Y.; Zhang, L.; Zhou, B.; Wei, Z.; Wang, D.; Lu, W.; Jia, J.; Tao, L.; Wang, T.; Wang, S. Coupling Fe(II)/Fe(III) Redox Mediated SO_2 Conversion with Hydrogen Production. *Adv. Funct. Mater.* **2023**, *33* (10), No. 2212479.
(40) Lee, J. E.; Ok, Y. S.; Tsang, D. C. W.; Song, J.; Jung, S.-C.; Park, Y.-K. Recent advances in volatile organic compounds abatement by catalysis and catalytic hybrid processes: A critical review. *ci. Total Environ.* **2020**, *719*, No. 137405.
(41) Zhan, Y.; Ji, J.; Huang, H.; He, M.; Leung, D. Y. C.; Liu, S.; Shu, Y.; Feng, Q.; Xie, R.; Fang, R.; Ye, X. A facile VUV/H_2O system without auxiliary substances for efficient degradation of gaseous toluene. *Chem. Eng. J.* **2018**, *334*, 1422−1429.
(42) Zhang, S.; You, J.; Kennes, C.; Cheng, Z.; Ye, J.; Chen, D.; Chen, J.; Wang, L. Current advances of VOCs degradation by bioelectrochemical systems: A review. *Chem. Eng. J.* **2018**, *334*, 2625−2637.
(43) Li, C.; He, L.; Yao, X.; Yao, Z. Recent advances in the chemical oxidation of gaseous volatile organic compounds (VOCs) in liquid phase. *Chemosphere* **2022**, *295*, No. 133868.
(44) Gong, X.; Yang, X.; Zheng, H.; Wu, Z. Elimination of ethanethiol released from municipal wastes by absorption sequencing electrochemical oxidation. *Environ. Technol.* **2017**, *38* (13−14), 1708−1715.
(45) Gong, X.; Yang, J.; Feng, X.; Yang, X.; Zheng, H.; Wu, Z.; Hu, Q. Removal of thiophene in air stream by absorption combined with electrochemical oxidation. *J. Taiwan Inst. Chem. Eng.* **2018**, *84*, 173−178.
(46) Huang, L.-W.; Qiu, P.-L.; Chen, J. Y.; Chen, A.-G.; Liu, Y.-X. Removal of styrene in air stream by absorption combined with electrochemical oxidation. *Environ. Technol.* **2020**, *41* (16), 2140−2145.
(47) González-Pérez, O.; Muñoz-Morales, M.; Souza, F. L.; Sáez, C.; Cañizares, P.; Rodrigo, M. A. Jet electro-absorbers for the treatment of gaseous perchloroethylene wastes. *Chem. Eng. J.* **2020**, *395*, No. 125096.
(48) Wu, J.; Sun, W.; Cao, L.; Yang, J. Removal of highly concentrated toluene from flue gas by an anode-supported solid oxide fuel cell reactor to generate electricity. *Chem. Eng. J.* **2016**, *301*, 334−341.
(49) Tang, T.; Wang, Z.; Guan, J. Optimizing the Electrocatalytic Selectivity of Carbon Dioxide Reduction Reaction by Regulating the Electronic Structure of Single-Atom M-N-C Materials. *Adv. Funct. Mater.* **2022**, *32* (19), No. 2111504.
(50) Li, X.; Zhu, Q.-L. MOF-based materials for photo- and electrocatalytic CO_2 reduction. *EnergyChem.* **2020**, *2* (3), No. 100033.
(51) Zhu, W.; Zhang, Y.-J.; Zhang, H.; Lv, H.; Li, Q.; Michalsky, R.; Peterson, A. A.; Sun, S. Active and Selective Conversion of CO_2 to CO on Ultrathin Au Nanowires. *J. Am. Chem. Soc.* **2014**, *136* (46), 16132−16135.
(52) Mistry, H.; Reske, R.; Zeng, Z.; Zhao, Z.-J.; Greeley, J.; Strasser, P.; Cuenya, B. R. Exceptional Size-Dependent Activity Enhancement in the Electroreduction of CO_2 over Au Nanoparticles. *J. Am. Chem. Soc.* **2014**, *136* (47), 16473−16476.
(53) Gao, Z.-H.; Wei, K.; Wu, T.; Dong, J.; Jiang, D.-e.; Sun, S.; Wang, L.-S. A Heteroleptic Gold Hydride Nanocluster for Efficient and Selective Electrocatalytic Reduction of CO_2 to CO. *J. Am. Chem. Soc.* **2022**, *144* (12), 5258−5262.
(54) Wang, G.; Chen, J.; Ding, Y.; Cai, P.; Yi, L.; Li, Y.; Tu, C.; Hou, Y.; Wen, Z.; Dai, L. Electrocatalysis for CO_2 conversion: from fundamentals to value-added products. *Chem. Soc. Rev.* **2021**, *50* (8), 4993−5061.
(55) Li, Z.; Li, X.; Wang, R.; Campos Mata, A.; Gerke, C. S.; Xiang, S.; Mathur, A.; Zhang, L.; Lin, D.-Z.; Li, T.; Jayarapu, K. N.; Liu, A.; Gupta, L.; Frenkel, A. I.; Thoi, V. S.; Ajayan, P. M.; Roy, S.; Liu, Y.; Liu, Y. Electro-activated indigos intensify ampere-level CO_2 reduction to CO on silver catalysts. *Nat. Commun.* **2025**, *16* (1), 3206.
(56) Li, X.; Zeng, Y.; Tung, C.-W.; Lu, Y.-R.; Baskaran, S.; Hung, S.-F.; Wang, S.; Xu, C.-Q.; Wang, J.; Chan, T.-S.; Chen, H. M.; Jiang, J.; Yu, Q.; Huang, Y.; Li, J.; Zhang, T.; Liu, B. Unveiling the In Situ Generation of a Monovalent Fe(I) Site in the Single-Fe-Atom Catalyst for Electrochemical CO_2 Reduction. *ACS Catal.* **2021**, *11* (12), 7292−7301.
(57) Liu, S.; Jin, M.; Sun, J.; Qin, Y.; Gao, S.; Chen, Y.; Zhang, S.; Luo, J.; Liu, X. Coordination environment engineering to boost electrocatalytic CO_2 reduction performance by introducing boron into single-Fe-atomic catalyst. *Chem. Eng. J.* **2022**, *437*, No. 135294.
(58) Guo, Y.; Yao, S.; Xue, Y.; Hu, X.; Cui, H.; Zhou, Z. Nickel single-atom catalysts intrinsically promoted by fast pyrolysis for selective electroreduction of CO_2 into CO. *Appl. Catal. B Environ.* **2022**, *304*, No. 120997.
(59) Pan, Y.; Lin, R.; Chen, Y.; Liu, S.; Zhu, W.; Cao, X.; Chen, W.; Wu, K.; Cheong, W.-C.; Wang, Y.; Zheng, L.; Luo, J.; Lin, Y.; Liu, Y.; Liu, C.; Li, J.; Lu, Q.; Chen, X.; Wang, D.; Peng, Q.; Chen, C.; Li, Y.

Design of Single-Atom Co−N5 Catalytic Site: A Robust Electrocatalyst for CO_2 Reduction with Nearly 100% CO Selectivity and Remarkable Stability. *J. Am. Chem. Soc.* **2018**, *140* (12), 4218−4221.

(60) Wang, Q.; Luo, T.; Cao, X.; Gong, Y.; Liu, Y.; Xiao, Y.; Li, H.; Gröbmeyer, F.; Lu, Y.-R.; Chan, T.-S.; Ma, C.; Liu, K.; Fu, J.; Zhang, S.; Liu, C.; Lin, Z.; Chai, L.; Cortes, E.; Liu, M. Lanthanide single-atom catalysts for efficient CO_2-to-CO electroreduction. *Nat. Commun.* **2025**, *16* (1), 2985.

(61) Rong, X.; Wang, H.-J.; Lu, X.-L.; Si, R.; Lu, T.-B. Controlled Synthesis of a Vacancy-Defect Single-Atom Catalyst for Boosting CO_2 Electroreduction. *Angew. Chem., Int. Ed.* **2020**, *59* (5), 1961−1965.

(62) Yang, H.; Shang, L.; Zhang, Q.; Shi, R.; Waterhouse, G. I. N.; Gu, L.; Zhang, T. A universal ligand mediated method for large scale synthesis of transition metal single atom catalysts. *Nat. Commun.* **2019**, *10* (1), 4585.

(63) Grasemann, M.; Laurenczy, G. Formic acid as a hydrogen source − recent developments and future trends. *Energy Environ. Sci.* **2012**, *5* (8), 8171−8181.

(64) Kortlever, R.; Shen, J.; Schouten, K. J. P.; Calle-Vallejo, F.; Koper, M. T. M. Catalysts and Reaction Pathways for the Electrochemical Reduction of Carbon Dioxide. *J. Phys. Chem. Lett.* **2015**, *6* (20), 4073−4082.

(65) Wang, J.; Deng, D.; Wu, Q.; Liu, M.; Wang, Y.; Jiang, J.; Zheng, X.; Zheng, H.; Bai, Y.; Chen, Y.; Xiong, X.; Lei, Y. Insight on Atomically Dispersed Cu Catalysts for Electrochemical CO_2 Reduction. *ACS Nano* **2023**, *17* (19), 18688−18705.

(66) Jiang, Z.; Wang, T.; Pei, J.; Shang, H.; Zhou, D.; Li, H.; Dong, J.; Wang, Y.; Cao, R.; Zhuang, Z.; Chen, W.; Wang, D.; Zhang, J.; Li, Y. Discovery of main group single Sb−N_4 active sites for CO_2 electroreduction to formate with high efficiency. *Energy Environ. Sci.* **2020**, *13* (9), 2856−2863.

(67) Peng, B.; She, H.; Wei, Z.; Sun, Z.; Deng, Z.; Sun, Z.; Chen, W. Sulfur-doping tunes p-d orbital coupling over asymmetric Zn-Sn dual-atom for boosting CO_2 electroreduction to formate. *Nat. Commun.* **2025**, *16* (1), 2217.

(68) Wang, Z.; Liu, D.; Xia, C.; Shi, X.; Zhou, Y.; Liu, Q.; Huang, J.; Wu, H.; Zhu, D.; Zhang, S.; Li, J.; Deng, P.; Vasenko, A. S.; Xia, B. Y.; Tian, X. Tip carbon encapsulation customizes cationic enrichment and valence stabilization for low K+ acidic CO_2 electroreduction. *Nat. Commun.* **2025**, *16* (1), 1754.

(69) Zhang, M.; Wei, W. B.; Zhou, S. H.; Ma, D. D.; Cao, A. H.; Wu, X. T.; Zhu, Q. L. Engineering a conductive network of atomically thin bismuthene with rich defects enables CO_2 reduction to formate with industry-compatible current densities and stability. *Energy Environ. Sci.* **2021**, *14* (9), 4998−5008.

(70) Han, N.; Wang, Y.; Yang, H.; Deng, J.; Wu, J.; Li, Y.; Li, Y. Ultrathin bismuth nanosheets from in situ topotactic transformation for selective electrocatalytic CO_2 reduction to formate. *Nat. Commun.* **2018**, *9* (1), 1320.

(71) Lee, C. W.; Hong, J. S.; Yang, K. D.; Jin, K.; Lee, J. H.; Ahn, H.-Y.; Seo, H.; Sung, N.-E.; Nam, K. T. Selective Electrochemical Production of Formate from Carbon Dioxide with Bismuth-Based Catalysts in an Aqueous Electrolyte. *ACS Catal.* **2018**, *8* (2), 931−937.

(72) Zhang, Y.; Zhang, X.; Ling, Y.; Li, F.; Bond, A. M.; Zhang, J. Controllable Synthesis of Few-Layer Bismuth Subcarbonate by Electrochemical Exfoliation for Enhanced CO_2 Reduction Performance. *Angew. Chem., Int. Ed.* **2018**, *57* (40), 13283−13287.

(73) Lin, L.; He, X.; Zhang, X.-G.; Ma, W.; Zhang, B.; Wei, D.; Xie, S.; Zhang, Q.; Yi, X.; Wang, Y. A Nanocomposite of Bismuth Clusters and $Bi_2O_2CO_3$ Sheets for Highly Efficient Electrocatalytic Reduction of CO_2 to Formate. *Angew. Chem., Int. Ed.* **2023**, *62* (3), No. e202214959.

(74) Zhu, J.; Li, J.; Lu, R.; Yu, R.; Zhao, S.; Li, C.; Lv, L.; Xia, L.; Chen, X.; Cai, W.; Meng, J.; Zhang, W.; Pan, X.; Hong, X.; Dai, Y.; Mao, Y.; Li, J.; Zhou, L.; He, G.; Pang, Q.; Zhao, Y.; Xia, C.; Wang, Z.; Dai, L.; Mai, L. Surface passivation for highly active, selective, stable, and scalable CO_2 electroreduction. *Nat. Commun.* **2023**, *14* (1), 4670.

(75) Liu, M.; Wang, Y.-R.; Ding, H.-M.; Lu, M.; Gao, G.-K.; Dong, L.-Z.; Li, Q.; Chen, Y.; Li, S.-L.; Lan, Y.-Q. Self-assembly of anthraquinone covalent organic frameworks as 1D superstructures for highly efficient CO_2 electroreduction to CH_4. *Sci. Bull.* **2021**, *66* (16), 1659−1668.

(76) Chen, X.; Lu, R.; Li, C.; Luo, W.; Yu, R.; Zhu, J.; Lv, L.; Dai, Y.; Gong, S.; Zhou, Y.; Xiong, W.; Wu, J.; Cai, H.; Wu, X.; Deng, Z.; Xing, B.; Su, L.; Wang, F.; Chao, F.; Chen, W.; Xia, C.; Wang, Z.; Mai, L. Activating inert non-defect sites in Bi catalysts using tensile strain engineering for highly active CO_2 electroreduction. *Nat. Commun.* **2025**, *16* (1), 1927.

(77) Qu, J.; Zhang, X.; Wang, Y.; Xie, C. Electrochemical reduction of CO_2 on RuO_2/TiO_2 nanotubes composite modified Pt electrode. *Electrochim. Acta* **2005**, *50* (16), 3576−3580.

(78) Shironita, S.; Karasuda, K.; Sato, K.; Umeda, M. Methanol generation by CO_2 reduction at a Pt−Ru/C electrocatalyst using a membrane electrode assembly. *J. Power Sources* **2013**, *240*, 404−410.

(79) Zhang, W.; Qin, Q.; Dai, L.; Qin, R.; Zhao, X.; Chen, X.; Ou, D.; Chen, J.; Chuong, T. T.; Wu, B.; Zheng, N. Electrochemical Reduction of Carbon Dioxide to Methanol on Hierarchical Pd/SnO_2 Nanosheets with Abundant Pd−O−Sn Interfaces. *Angew. Chem., Int. Ed.* **2018**, *57* (30), 9475−9479.

(80) Yang, H.; Wu, Y.; Li, G.; Lin, Q.; Hu, Q.; Zhang, Q.; Liu, J.; He, C. Scalable Production of Efficient Single-Atom Copper Decorated Carbon Membranes for CO_2 Electroreduction to Methanol. *J. Am. Chem. Soc.* **2019**, *141* (32), 12717−12723.

(81) Yang, D.; Zhu, Q.; Chen, C.; Liu, H.; Liu, Z.; Zhao, Z.; Zhang, X.; Liu, S.; Han, B. Selective electroreduction of carbon dioxide to methanol on copper selenide nanocatalysts. *Nat. Commun.* **2019**, *10* (1), 677.

(82) Li, P.; Bi, J.; Liu, J.; Zhu, Q.; Chen, C.; Sun, X.; Zhang, J.; Han, B. In situ dual doping for constructing efficient CO_2-to-methanol electrocatalysts. *Nat. Commun.* **2022**, *13* (1), 1965.

(83) Li, B.; Liu, L.; Yue, M.; Niu, Q.; Li, M.; Zhang, T.; Xie, W.; Wang, Q. Status and challenges for CO_2 electroreduction to CH_4: advanced catalysts and enhanced strategies. *Green Chem.* **2024**, *26* (1), 103−121.

(84) Fan, M.; Miao, R. K.; Ou, P.; Xu, Y.; Lin, Z.-Y.; Lee, T.-J.; Hung, S.-F.; Xie, K.; Huang, J. E.; Ni, W.; Li, J.; Zhao, Y.; Ozden, A.; O'Brien, C. P.; Chen, Y.; Xiao, Y. C.; Liu, S.; Wicks, J.; Wang, X.; Abed, J.; Shirzadi, E.; Sargent, E. H.; Sinton, D. Single-site decorated copper enables energy- and carbon-efficient CO_2 methanation in acidic conditions. *Nat. Commun.* **2023**, *14* (1), 3314.

(85) Zhao, P.; Jiang, H.; Shen, H.; Yang, S.; Gao, R.; Guo, Y.; Zhang, Q.; Zhang, H. Construction of Low-Coordination Cu−C_2 Single-Atoms Electrocatalyst Facilitating the Efficient Electrochemical CO_2 Reduction to Methane. *Angew. Chem., Int. Ed.* **2023**, *62* (49), No. e202314121.

(86) Zhang, Y.; Chen, F.; Yang, X.; Guo, Y.; Zhang, X.; Dong, H.; Wang, W.; Lu, F.; Lu, Z.; Liu, H.; Liu, H.; Xiao, Y.; Cheng, Y. Electronic metal-support interaction modulates Cu electronic structures for CO_2 electroreduction to desired products. *Nat. Commun.* **2025**, *16* (1), 1956.

(87) Han, L.; Song, S.; Liu, M.; Yao, S.; Liang, Z.; Cheng, H.; Ren, Z.; Liu, W.; Lin, R.; Qi, G.; Liu, X.; Wu, Q.; Luo, J.; Xin, H. L. Stable and Efficient Single-Atom Zn Catalyst for CO_2 Reduction to CH_4. *J. Am. Chem. Soc.* **2020**, *142* (29), 12563−12567.

(88) Liu, J.; Li, P.; Jia, S.; Wang, Y.; Jing, L.; Liu, Z.; Zhang, J.; Qian, Q.; Kang, X.; Sun, X.; Zhu, Q.; Han, B. Electrocatalytic CO_2 hydrogenation to C_{2+} alcohols catalysed by Pr−Cu oxide hetero-interfaces. *Nat. Synth.* **2025**, *4*, 730.

(89) Rahaman, M.; Dutta, A.; Zanetti, A.; Broekmann, P. Electrochemical Reduction of CO_2 into Multicarbon Alcohols on Activated Cu Mesh Catalysts: An Identical Location (IL) Study. *ACS Catal.* **2017**, *7* (11), 7946−7956.

(90) Adegoke, K. A.; Adegoke, R. O.; Ibrahim, A. O.; Adegoke, S. A.; Bello, O. S. Electrocatalytic conversion of CO_2 to hydrocarbon and alcohol products: Realities and prospects of Cu-based materials. *Sustainable Mater. Technol.* **2020**, *25*, No. e00200.

https://doi.org/10.1021/acs.est.5c06634
Environ. Sci. Technol. 2025, 59, 24177−24196

(91) Gu, Z.; Shen, H.; Chen, Z.; Yang, Y.; Yang, C.; Ji, Y.; Wang, Y.; Zhu, C.; Liu, J.; Li, J.; Sham, T.-K.; Xu, X.; Zheng, G. Efficient Electrocatalytic CO_2 Reduction to C_{2+} Alcohols at Defect-Site-Rich Cu Surface. *Joule* **2021**, *5* (2), 429−440.

(92) Liu, K.; Shen, H.; Sun, Z.; Zhou, Q.; Liu, G.; Sun, Z.; Chen, W.; Gao, X.; Chen, P. Transient pulsed discharge preparation of graphene aerogel supports asymmetric Cu cluster catalysts promote CO_2 electroreduction. *Nat. Commun.* **2025**, *16* (1), 1203.

(93) Gao, J.; Bahmanpour, A.; Kröcher, O.; Zakeeruddin, S. M.; Ren, D.; Grätzel, M. Electrochemical synthesis of propylene from carbon dioxide on copper nanocrystals. *Nat. Chem.* **2023**, *15* (5), 705−713.

(94) Fang, M.; Wang, M.; Wang, Z.; Zhang, Z.; Zhou, H.; Dai, L.; Zhu, Y.; Jiang, L. Hydrophobic, Ultrastable $Cu^{\delta+}$ for Robust CO_2 Electroreduction to C_2 Products at Ampere-Current Levels. *J. Am. Chem. Soc.* **2023**, *145* (20), 11323−11332.

(95) Feng, J.; Wu, L.; Liu, S.; Xu, L.; Song, X.; Zhang, L.; Zhu, Q.; Kang, X.; Sun, X.; Han, B. Improving CO_2-to-C_{2+} Product Electroreduction Efficiency via Atomic Lanthanide Dopant-Induced Tensile-Strained CuO_x Catalysts. *J. Am. Chem. Soc.* **2023**, *145* (17), 9857−9866.

(96) Zhou, Y.; Yao, Y.; Zhao, R.; Wang, X.; Fu, Z.; Wang, D.; Wang, H.; Zhao, L.; Ni, W.; Yang, Z.; Yan, Y.-M. Stabilization of Cu+ via Strong Electronic Interaction for Selective and Stable CO_2 Electroreduction. *Angew. Chem., Int. Ed.* **2022**, *61* (31), No. e202205832.

(97) Tan, Z.; Zhang, J.; Yang, Y.; Zhong, J.; Zhao, Y.; Hu, J.; Han, B.; Chen, Z. Alkaline Ionic Liquid Microphase Promotes Deep Reduction of CO_2 on Copper. *J. Am. Chem. Soc.* **2023**, *145* (40), 21983−21990.

(98) Tan, Z.; Zhang, J.; Yang, Y.; Zhong, J.; Zhao, Y.; Teng, Y.; Han, B.; Chen, Z. Polymeric ionic liquid promotes acidic electrocatalytic CO_2 conversion to multicarbon products with ampere level current on Cu. *Nat. Commun.* **2025**, *16* (1), 1843.

(99) Li, Y.; Cheng, C.; Han, S.; Huang, Y.; Du, X.; Zhang, B.; Yu, Y. Electrocatalytic Reduction of Low-Concentration Nitric Oxide into Ammonia over Ru Nanosheets. *ACS Energy Lett.* **2022**, *7* (3), 1187−1194.

(100) Mou, T.; Liang, J.; Ma, Z.; Zhang, L.; Lin, Y.; Li, T.; Liu, Q.; Luo, Y.; Liu, Y.; Gao, S.; Zhao, H.; Asiri, A. M.; Ma, D.; Sun, X. High-efficiency electrohydrogenation of nitric oxide to ammonia on a Ni_2P nanoarray under ambient conditions. *J. Mater. Chem. A* **2021**, *9* (43), 24268−24275.

(101) Long, J.; Chen, S.; Zhang, Y.; Guo, C.; Fu, X.; Deng, D.; Xiao, J. Direct Electrochemical Ammonia Synthesis from Nitric Oxide. *Angew. Chem., Int. Ed.* **2020**, *59* (24), 9711−9718.

(102) Zacharia, I. G.; Deen, W. M. Diffusivity and Solubility of Nitric Oxide in Water and Saline. *Ann. Biomed. Eng.* **2005**, *33* (2), 214−222.

(103) Guo, Q.; He, Y.; Sun, T.; Wang, Y.; Jia, J. Simultaneous removal of NO_x and SO_2 from flue gas using combined Na_2SO_3 assisted electrochemical reduction and direct electrochemical reduction. *J. Hazard. Mater.* **2014**, *276*, 371−376.

(104) Kim, D.; Shin, D.; Heo, J.; Lim, H.; Lim, J.-A.; Jeong, H. M.; Kim, B.-S.; Heo, I.; Oh, I.; Lee, B.; Sharma, M.; Lim, H.; Kim, H.; Kwon, Y. Unveiling Electrode−Electrolyte Design-Based NO Reduction for NH_3 Synthesis. *ACS Energy Lett.* **2020**, *5* (11), 3647−3656.

(105) Xiong, Y.; Li, Y.; Wan, S.; Yu, Y.; Zhang, S.; Zhong, Q. Ferrous-based electrolyte for simultaneous NO absorption and electroreduction to NH_3 using Au/rGO electrode. *J. Hazard. Mater.* **2022**, *430*, No. 128451.

(106) Wu, Q.; Wei, W.; Lv, X.; Wang, Y.; Huang, B.; Dai, Y. Cu@g-C3N4: An Efficient Single-Atom Electrocatalyst for NO Electrochemical Reduction with Suppressed Hydrogen Evolution. *J. Phys. Chem. C* **2019**, *123* (51), 31043−31049.

(107) Chen, L.; Sun, W.; Xu, Z.; Hao, M.; Li, B.; Liu, X.; Ma, J.; Wang, L.; Li, C.; Wang, W. Ultrafine Cu nanoparticles decorated porous TiO_2 for high-efficient electrocatalytic reduction of NO to synthesize NH_3. *Ceram. Int.* **2022**, *48* (15), 21151−21161.

(108) Yang, W.; Liu, H.; Chang, X.; Zhang, Y.; Cai, Y.; Li, Y.; Cui, Y.; Xu, B.; Yu, L.; Cui, X.; Deng, D. Electrosynthesis of NH_3 from NO with ampere-level current density in a pressurized electrolyzer. *Nat. Commun.* **2025**, *16* (1), 1257.

(109) Wang, D.; Chen, Z.-W.; Gu, K.; Chen, C.; Liu, Y.; Wei, X.; Singh, C. V.; Wang, S. Hexagonal Cobalt Nanosheets for High-Performance Electrocatalytic NO Reduction to NH_3. *J. Am. Chem. Soc.* **2023**, *145* (12), 6899−6904.

(110) Muthusamy, T.; Sethuram Markandaraj, S.; Shanmugam, S. Nickel nanoparticles wrapped in N-doped carbon nanostructures for efficient electrochemical reduction of NO to NH_3. *J. Mater. Chem. A* **2022**, *10* (12), 6470−6474.

(111) Wei, T.; Bao, H.; Wang, X.; Zhang, S.; Liu, Q.; Luo, J.; Liu, X. Ionic Liquid-Assisted Electrocatalytic NO Reduction to NH_3 by P-Doped MoS_2. *ChemCatChem.* **2023**, *15* (3), No. e202201411.

(112) Chen, K.; Zhang, G.; Li, X.; Zhao, X.; Chu, K. Electrochemical NO reduction to NH_3 on Cu single atom catalyst. *Nano Res.* **2023**, *16* (4), 5857−5863.

(113) Peng, X.; Mi, Y.; Bao, H.; Liu, Y.; Qi, D.; Qiu, Y.; Zhuo, L.; Zhao, S.; Sun, J.; Tang, X.; Luo, J.; Liu, X. Ambient electrosynthesis of ammonia with efficient denitration. *Nano Energy* **2020**, *78*, No. 105321.

(114) Chen, K.; Wang, J.; Zhang, H.; Ma, D.; Chu, K. Self-Tandem Electrocatalytic NO Reduction to NH_3 on a W Single-Atom Catalyst. *Nano Lett.* **2023**, *23* (5), 1735−1742.

(115) Lou, Z.; Zhang, H.; Zhao, X.; Liu, Q.; Liang, M.; Wang, H.; Yang, H.; Cai, B.; Lu, J.; Cui, Y.; Wu, J.; Teng, F.; Lu, X.; Yuan, W.; Liu, M. High-resolution mapping of CH_4/N_2O emissions from industrialization-related anthropogenic sources in China. *Natl. Sci. Rev.* **2025**, *12* (4), No. nwae481.

(116) Martinez, J. L.; Schneider, J. E.; Anferov, S. W.; Anderson, J. S. Electrochemical Reduction of N_2O with a Molecular Copper Catalyst. *ACS Catal.* **2023**, *13* (19), 12673−12680.

(117) Li, Z.; Wu, Y.; Wang, H.; Wu, Z.; Wu, X. High-Efficiency Electrocatalytic Reduction of N_2O with Single-Atom Cu Supported on Nitrogen-Doped Carbon. *Environ. Sci. Technol.* **2024**, *58* (20), 8976−8987.

(118) Wu, Y.; Wang, H.; Xiao, F.-S.; Wu, Z. Gadolinium-Mediated Oxygen Affinity Induced Efficient Covalorization of CH_4 and N_2O in an Ir−Gd_2O_3 Single-Atom Catalyst. *J. Am. Chem. Soc.* **2025**, *147* (29), 25787−25798.

(119) Huang, Y.; Yang, R.; Wang, C.; Meng, N.; Shi, Y.; Yu, Y.; Zhang, B. Direct Electrosynthesis of Urea from Carbon Dioxide and Nitric Oxide. *ACS Energy Lett.* **2022**, *7* (1), 284−291.

(120) Guo, Q.; Sun, T.; Wang, Y.; He, Y.; Jia, J. Spray Absorption and Electrochemical Reduction of Nitrogen Oxides from Flue Gas. *Environ. Sci. Technol.* **2013**, *47* (16), 9514−9522.

(121) Yang, F.; Liang, C.; Zhou, W.; Zhao, W.; Li, P.; Hua, Z.; Yu, H.; Chen, S.; Deng, S.; Li, J.; Lam, Y. M.; Wang, J. Oxide-Derived Bismuth as an Efficient Catalyst for Electrochemical Reduction of Flue Gas. *Small* **2023**, *19* (30), No. 2300417.

(122) Raju, T.; Chung, S. J.; Pillai, K. C.; Moon, I.-S. Simultaneous Removal of NO_x and SO_2: A Promising Ag(II)/Ag(I) Based Mediated Electrochemical Oxidation System. *CLEAN − Soil Air Water* **2008**, *36* (5−6), 476−481.

(123) Chandrasekara Pillai, K.; Chung, S. J.; Raju, T.; Moon, I.-S. Experimental aspects of combined NO_x and SO_2 removal from flue-gas mixture in an integrated wet scrubber-electrochemical cell system. *Chemosphere* **2009**, *76* (5), 657−664.

(124) Hibino, T. Electrochemical Removal of NO and CH_4 from Oxidizing Atmosphere. *Chem. Lett.* **1994**, *23* (5), 927−930.

(125) Ma, J.; Mao, K.; Low, J.; Wang, Z.; Xi, D.; Zhang, W.; Ju, H.; Qi, Z.; Long, R.; Wu, X.; Song, L.; Xiong, Y. Efficient Photoelectrochemical Conversion of Methane into Ethylene Glycol by WO_3 Nanobar Arrays. *Angew. Chem., Int. Ed.* **2021**, *60* (17), 9357−9361.

(126) Liang, S.; Altaf, N.; Huang, L.; Gao, Y.; Wang, Q. Electrolytic cell design for electrochemical CO_2 reduction. *J. CO2 Util.* **2020**, *35*, 90−105.

https://doi.org/10.1021/acs.est.5c06634
Environ. Sci. Technol. 2025, 59, 24177−24196

(127) Burdyny, T.; Smith, W. A. CO_2 reduction on gas-diffusion electrodes and why catalytic performance must be assessed at commercially-relevant conditions. *Energy Environ. Sci.* **2019**, *12* (5), 1442−1453.

(128) Xing, Z.; Hu, L.; Ripatti, D. S.; Hu, X.; Feng, X. Enhancing carbon dioxide gas-diffusion electrolysis by creating a hydrophobic catalyst microenvironment. *Nat. Commun.* **2021**, *12* (1), 136.

(129) Chen, Z.; Zhang, X.; Liu, W.; Jiao, M.; Mou, K.; Zhang, X.; Liu, L. Amination strategy to boost the CO_2 electroreduction current density of M−N/C single-atom catalysts to the industrial application level. *Energy Environ. Sci.* **2021**, *14* (4), 2349−2356.

(130) Ma, L.; Liu, H.; Mei, B.; Chen, J.; Cheng, Q.; Ma, J.; Yang, B.; Li, Q.; Yang, H. Cu supraparticles with enhanced mass transfer and abundant C-C coupling sites achieving ampere-level CO_2-to-C_{2+} electrosynthesis. *Nat. Commun.* **2025**, *16* (1), 3421.

(131) Shi, R.; Guo, J.; Zhang, X.; Waterhouse, G. I. N.; Han, Z.; Zhao, Y.; Shang, L.; Zhou, C.; Jiang, L.; Zhang, T. Efficient wettability-controlled electroreduction of CO_2 to CO at Au/C interfaces. *Nat. Commun.* **2020**, *11* (1), 3028.

(132) Li, J.; Chen, G.; Zhu, Y.; Liang, Z.; Pei, A.; Wu, C.-L.; Wang, H.; Lee, H. R.; Liu, K.; Chu, S.; Cui, Y. Efficient electrocatalytic CO_2 reduction on a three-phase interface. *Nat. Catal.* **2018**, *1* (8), 592−600.

(133) Cheon, S.; Kim, W. J.; Kim, D. Y.; Kwon, Y.; Han, J.-I. Electro-synthesis of Ammonia from Dilute Nitric Oxide on a Gas Diffusion Electrode. *ACS Energy Lett.* **2022**, *7* (3), 958−965.

(134) Rocha, R. S.; Camargo, L. M.; Lanza, M. R. V.; Bertazzoli, R. A Feasibility Study of the Electro-recycling of Greenhouse Gases: Design and Characterization of a (TiO_2/RuO_2)/PTFE Gas Diffusion Electrode for the Electrosynthesis of Methanol from Methane. *Electrocatalysis* **2010**, *1* (4), 224−229.

(135) Rocha, R. S.; Reis, R. M.; Lanza, M. R. V.; Bertazzoli, R. Electrosynthesis of methanol from methane: The role of V_2O_5 in the reaction selectivity for methanol of a $TiO_2/RuO_2/V_2O_5$ gas diffusion electrode. *Electrochim. Acta* **2013**, *87*, 606−610.

(136) Wakerley, D.; Lamaison, S.; Wicks, J.; Clemens, A.; Feaster, J.; Corral, D.; Jaffer, S. A.; Sarkar, A.; Fontecave, M.; Duoss, E. B.; Baker, S.; Sargent, E. H.; Jaramillo, T. F.; Hahn, C. Gas diffusion electrodes, reactor designs and key metrics of low-temperature CO_2 electrolysers. *Nat. Energy* **2022**, *7* (2), 130−143.

(137) Xu, T.; Yang, H.; Lu, T.; Zhong, R.; Lv, J.-J.; Zhu, S.; Zhang, M.; Wang, Z.-J.; Yuan, Y.; Li, J.; Wang, J.; Jin, H.; Pan, S.; Wang, X.; Cheng, T.; Wang, S. Microenvironment engineering by targeted delivery of Ag nanoparticles for boosting electrocatalytic CO_2 reduction reaction. *Nat. Commun.* **2025**, *16* (1), 977.

(138) Verma, S.; Hamasaki, Y.; Kim, C.; Huang, W.; Lu, S.; Jhong, H.-R. M.; Gewirth, A. A.; Fujigaya, T.; Nakashima, N.; Kenis, P. J. A. Insights into the Low Overpotential Electroreduction of CO_2 to CO on a Supported Gold Catalyst in an Alkaline Flow Electrolyzer. *ACS Energy Lett.* **2018**, 3 (1), 193−198.

(139) Yang, H.; Lin, Q.; Zhang, C.; Yu, X.; Cheng, Z.; Li, G.; Hu, Q.; Ren, X.; Zhang, Q.; Liu, J.; He, C. Carbon dioxide electroreduction on single-atom nickel decorated carbon membranes with industry compatible current densities. *Nat. Commun.* **2020**, *11* (1), 593.

(140) Shi, R.; Zhang, T. Single-atom Ni integrated gas diffusion electrode for high performance carbon dioxide electroreduction. *Sci. Bull.* **2020**, *65* (9), 696−697.

(141) Weng, L.-C.; Bell, A. T.; Weber, A. Z. Towards membrane-electrode assembly systems for CO_2 reduction: a modeling study. *Energy Environ. Sci.* **2019**, *12* (6), 1950−1968.

(142) Ren, S.; Joulié, D.; Salvatore, D.; Torbensen, K.; Wang, M.; Robert, M.; Berlinguette, C. P. Molecular electrocatalysts can mediate fast, selective CO_2 reduction in a flow cell. *Science* **2019**, *365* (6451), 367−369.

(143) Fornaciari, J. C.; Primc, D.; Kawashima, K.; Wygant, B. R.; Verma, S.; Spanu, L.; Mullins, C. B.; Bell, A. T.; Weber, A. Z. A Perspective on the Electrochemical Oxidation of Methane to Methanol in Membrane Electrode Assemblies. *ACS Energy Lett.* **2020**, *5* (9), 2954−2963.

(144) Lee, B.; Hibino, T. Efficient and selective formation of methanol from methane in a fuel cell-type reactor. *J. Catal.* **2011**, *279* (2), 233−240.

(145) Hao, S.; Elgazzar, A.; Ravi, N.; Wi, T.-U.; Zhu, P.; Feng, Y.; Xia, Y.; Chen, F.-Y.; Shan, X.; Wang, H. Improving the operational stability of electrochemical CO_2 reduction reaction via salt precipitation understanding and management. *Nat. Energy* **2025**, *10* (2), 266−277.

(146) Ye, N.; Wang, K.; Tan, Y.; Qian, Z.; Guo, H.; Shang, C.; Lin, Z.; Huang, Q.; Liu, Y.; Li, L.; Gu, Y.; Han, Y.; Zhou, C.; Luo, M.; Guo, S. Industrial-level CO_2 to formate conversion on Turing-structured electrocatalysts. *Nat. Synth.* **2025**, *4*, 799.

(147) Jiao, F.; Xu, B. Electrochemical Ammonia Synthesis and Ammonia Fuel Cells. *Adv. Mater.* **2019**, *31* (31), No. 1805173.

(148) Lai, W.; Qiao, Y.; Zhang, J.; Lin, Z.; Huang, H. Design strategies for markedly enhancing energy efficiency in the electrocatalytic CO_2 reduction reaction. *Energy Environ. Sci.* **2022**, *15* (9), 3603−3629.

(149) Sun, J. W.; Fu, H. Q.; Liu, P. F.; Chen, A.; Liu, P.; Yang, H. G.; Zhao, H. Advances and challenges in scalable carbon dioxide electrolysis. *EES Catal.* **2023**, *1* (6), 934−949.

(150) Kato, N.; Mizuno, S.; Shiozawa, M.; Nojiri, N.; Kawai, Y.; Fukumoto, K.; Morikawa, T.; Takeda, Y. A large-sized cell for solar-driven CO_2 conversion with a solar-to-formate conversion efficiency of 7.2%. *Joule* **2021**, *5* (3), 687−705.

(151) He, X.; Lin, L.; Li, X.; Zhu, M.; Zhang, Q.; Xie, S.; Mei, B.; Sun, F.; Jiang, Z.; Cheng, J.; Wang, Y. Roles of copper(I) in water-promoted CO_2 electrolysis to multi-carbon compounds. *Nat. Commun.* **2024**, *15* (1), 9923.

(152) Yuan, L.; Zeng, S.; Zhang, X.; Ji, X.; Zhang, S. Advances and challenges of electrolyzers for large-scale CO_2 electroreduction. *Mater. Rep. Energy* **2023**, 3 (1), No. 100177.

(153) Lu, X.; Leung, D. Y. C.; Wang, H.; Maroto-Valer, M. M.; Xuan, J. A pH-differential dual-electrolyte microfluidic electrochemical cells for CO_2 utilization. *Renew. Energy* **2016**, *95*, 277−285.

(154) Whipple, D. T.; Finke, E. C.; Kenis, P. J. A. Microfluidic Reactor for the Electrochemical Reduction of Carbon Dioxide: The Effect of pH. *Electrochem. Solid-State Lett.* **2010**, *13* (9), B109.

(155) Verma, S.; Lu, X.; Ma, S.; Masel, R. I.; Kenis, P. J. A. The effect of electrolyte composition on the electroreduction of CO_2 to CO on Ag based gas diffusion electrodes. *Phys. Chem. Chem. Phys.* **2016**, *18* (10), 7075−7084.

(156) Xia, C.; Zhu, P.; Jiang, Q.; Pan, Y.; Liang, W.; Stavitski, E.; Alshareef, H. N.; Wang, H. Continuous production of pure liquid fuel solutions via electrocatalytic CO_2 reduction using solid-electrolyte devices. *Nat. Energy* **2019**, *4* (9), 776−785.

(157) Fan, L.; Xia, C.; Zhu, P.; Lu, Y.; Wang, H. Electrochemical CO_2 reduction to high-concentration pure formic acid solutions in an all-solid-state reactor. *Nat. Commun.* **2020**, *11* (1), 3633.

(158) Zheng, T.; Liu, C.; Guo, C.; Zhang, M.; Li, X.; Jiang, Q.; Xue, W.; Li, H.; Li, A.; Pao, C.-W.; Xiao, J.; Xia, C.; Zeng, J. Copper-catalysed exclusive CO_2 to pure formic acid conversion via single-atom alloying. *Nat. Nanotechnol.* **2021**, *16* (12), 1386−1393.

(159) Elgazzar, A.; Wang, H. Beyond molecular transformations in electrochemical porous solid electrolyte reactors. *Nat. Chem. Eng.* **2025**, *2* (1), 3−7.

(160) Xue, S.; Gao, Y.; Wang, B.; Zhi, L. Effects of external physical fields on electrocatalysis. *Chem. Catal.* **2023**, *3*, No. 100762.

(161) Ma, J.; Mao, K.; Li, J.; Zhai, G.; Wu, D.; Liu, D.; Long, R.; Xiong, Y. Modulating Chloride Adsorption for Efficient Chloride-Mediated Methane Conversion over Tungsten Oxide Photoanode. *ACS Catal.* **2025**, *15* (8), 6058−6066.

(162) Mehmood, A.; Chae, S. Y.; Park, E. D. Photoelectrochemical Conversion of Methane into Value-Added Products. *Catalysts* **2021**, *11* (11), 1387.

(163) Ochedi, F. O.; Liu, D.; Yu, J.; Hussain, A.; Liu, Y. Photocatalytic, electrocatalytic and photoelectrocatalytic conversion

of carbon dioxide: a review. *Environ. Chem. Lett.* **2021**, *19* (2), 941−967.

(164) Li, S.; Shang, H.; Tao, Y.; Li, P.; Pan, H.; Wang, Q.; Zhang, S.; Jia, H.; Zhang, H.; Cao, J.; Zhang, B.; Zhang, R.; Li, G.; Zhang, Y.; Zhang, D.; Li, H. Hydroxyl Radical-Mediated Efficient Photoelectrocatalytic NO Oxidation with Simultaneous Nitrate Storage Using A Flow Photoanode Reactor. *Angew. Chem., Int. Ed.* **2023**, *62* (28), No. e202305538.

(165) Wang, X.; Gao, C.; Low, J.; Mao, K.; Duan, D.; Chen, S.; Ye, R.; Qiu, Y.; Ma, J.; Zheng, X.; Long, R.; Wu, X.; Song, L.; Zhu, J.; Xiong, Y. Efficient photoelectrochemical CO_2 conversion for selective acetic acid production. *Sci. Bull.* **2021**, *66* (13), 1296−1304.

(166) Nie, S.; Wu, L.; Wang, X. Electron-Delocalization-Stabilized Photoelectrocatalytic Coupling of Methane by NiO-Polyoxometalate Sub-1 nm Heterostructures. *J. Am. Chem. Soc.* **2023**, *145* (43), 23681−23690.

(167) Feng, G.; Wang, S.; Li, S.; Ge, R.; Feng, X.; Zhang, J.; Song, Y.; Dong, X.; Zhang, J.; Zeng, G.; Zhang, Q.; Ma, G.; Chuang, Y.-D.; Zhang, X.; Guo, J.; Sun, Y.; Wei, W.; Chen, W. Highly Selective Photoelectroreduction of Carbon Dioxide to Ethanol over Graphene/Silicon Carbide Composites. *Angew. Chem., Int. Ed.* **2023**, *62* (15), No. e202218664.

(168) Mei, X.; Bai, J.; Chen, S.; Zhou, M.; Jiang, P.; Zhou, C.; Fang, F.; Zhang, Y.; Li, J.; Long, M.; Zhou, B. Efficient SO_2 Removal and Highly Synergistic H_2O_2 Production Based on a Novel Dual-Function Photoelectrocatalytic System. *Environ. Sci. Technol.* **2020**, *54* (18), 11515−11525.

(169) Zhou, C.; Li, J.; Zhang, Y.; Bai, J.; Wang, P.; Zhang, B.; Zha, L.; Long, M.; Zhou, B. A novel $SO_3•^-$ mediated photoelectrocatalytic system based on MoS_2/Fe_2O_3 and CuNW@CF for the efficient treatment of sulfurous and nitrogenous oxides. *Appl. Catal. B Environ.* **2023**, *330*, No. 122579.

(170) Xiao, S.; Wan, Z.; Zhou, J.; Li, H.; Zhang, H.; Su, C.; Chen, W.; Li, G.; Zhang, D.; Li, H. Gas-Phase Photoelectrocatalysis for Breaking Down Nitric Oxide. *Environ. Sci. Technol.* **2019**, *53* (12), 7145−7154.

(171) Dai, W.; Tao, Y.; Zou, H.; Xiao, S.; Li, G.; Zhang, D.; Li, H. Gas-Phase Photoelectrocatalytic Oxidation of NO via TiO_2 Nanorod Array/FTO Photoanodes. *Environ. Sci. Technol.* **2020**, *54* (9), 5902−5912.

(172) Yang, B.; Zeng, J.; Zhang, Z.; Meng, L.; Shi, D.; Chen, L.; Huang, Y. Kinetic-boosted CO_2 electroreduction to formate via synergistic electric-thermal field on hierarchical bismuth with amorphous layer. *J. Energy Chem.* **2024**, *90*, 233.

(173) Chen, Y.; deGlee, B.; Tang, Y.; Wang, Z.; Zhao, B.; Wei, Y.; Zhang, L.; Yoo, S.; Pei, K.; Kim, J. H.; Ding, Y.; Hu, P.; Tao, F. F.; Liu, M. A robust fuel cell operated on nearly dry methane at 500 °C enabled by synergistic thermal catalysis and electrocatalysis. *Nat. Energy* **2018**, *3* (12), 1042−1050.

(174) Yang, B.; Liu, K.; Li, H.; Liu, C.; Fu, J.; Li, H.; Huang, J. E.; Ou, P.; Alkayyali, T.; Cai, C.; Duan, Y.; Liu, H.; An, P.; Zhang, N.; Li, W.; Qiu, X.; Jia, C.; Hu, J.; Chai, L.; Lin, Z.; Gao, Y.; Miyauchi, M.; Cortés, E.; Maier, S. A.; Liu, M. Accelerating CO_2 Electroreduction to Multicarbon Products via Synergistic Electric−Thermal Field on Copper Nanoneedles. *J. Am. Chem. Soc.* **2022**, *144* (7), 3039−3049.

(175) Yang, H.; Li, S.; Xu, Q. Efficient strategies for promoting the electrochemical reduction of CO_2 to C_{2+} products over Cu-based catalysts. *Chin. J. Catal.* **2023**, *48*, 32−65.

(176) Zhong, S.; Guo, X.; Zhou, A.; Chen, Z. a.; Jin, D.; Fan, M.; Ma, T. Fundamentals and Recent Progress in Magnetic Field Assisted CO_2 Capture and Conversion. *Small* **2024**, *20* (5), No. 2305533.

(177) Mitra, K.; Adalder, A.; Mandal, S.; Ghorai, U. K. Enhancing Electrochemical Reactivity with Magnetic Fields: Unraveling the Role of Magneto-Electrochemistry. *Small Methods* **2024**, *8* (7), No. 2301132.

(178) Zhang, Y.; Liang, C.; Wu, J.; Liu, H.; Zhang, B.; Jiang, Z.; Li, S.; Xu, P. Recent Advances in Magnetic Field-Enhanced Electrocatalysis. *ACS Appl. Energy Mater.* **2020**, *3* (11), 10303−10316.

(179) Woodward, J. R. Radical Pairs in Solution. *Prog. React. Kinet. Mech.* **2002**, *27* (3), 165−207.

(180) Silvi, B.; Savin, A. J. N. Classification of chemical bonds based on topological analysis of electron localization functions. *Nature* **1994**, *371* (6499), 683−686.

(181) Pan, H.; Jiang, X.; Wang, X.; Wang, Q.; Wang, M.; Shen, Y. Effective Magnetic Field Regulation of the Radical Pair Spin States in Electrocatalytic CO_2 Reduction. *J. Phys. Chem. Lett.* **2020**, *11* (1), 48−53.

(182) Hao, J.; Xie, S.; Huang, Q.; Ding, Z.; Sheng, H.; Zhang, C.; Yao, J. Spin-Enhanced C−C Coupling in CO_2 Electroreduction with Oxide-Derived Copper. *CCS Chem.* **2023**, *5* (9), 2046−2058.

(183) Wang, P.; Qu, Y.; Meng, X.; Tu, J.; Zheng, W.; Hu, L.; Chen, Q. A Strong Magnetic Field Alters the Activity and Selectivity of the CO_2RR by Restraining C−C Coupling. *Magnetochemistry* **2023**, *9*, 65.

(184) Kodaimati, M. S.; Gao, R.; Root, S. E.; Whitesides, G. M. Magnetic fields enhance mass transport during electrocatalytic reduction of CO_2. *Chem. Catal.* **2022**, *2* (4), 797−815.

(185) Bhargava, S. S.; Azmoodeh, D.; Chen, X.; Cofell, E. R.; Esposito, A. M.; Verma, S.; Gewirth, A. A.; Kenis, P. J. A. Decreasing the Energy Consumption of the CO_2 Electrolysis Process Using a Magnetic Field. *ACS Energy Lett.* **2021**, *6* (7), 2427−2433.

(186) Yin, H.; Dou, Y.; Chen, S.; Zhu, Z.; Liu, P.; Zhao, H. 2D Electrocatalysts for Converting Earth-Abundant Simple Molecules into Value-Added Commodity Chemicals: Recent Progress and Perspectives. *Adv. Mater.* **2020**, *32* (18), No. 1904870.

(187) Ou, H.; Wang, D.; Li, Y. How to select effective electrocatalysts: Nano or single atom? *Nano Select* **2021**, *2* (3), 492−511.

(188) Liu, Y.; Xiao, C.; Huang, P.; Cheng, M.; Xie, Y. Regulating the Charge and Spin Ordering of Two-Dimensional Ultrathin Solids for Electrocatalytic Water Splitting. *Chem.* **2018**, *4* (6), 1263−1283.

(189) Yin, Y.; Han, J.; Zhang, Y.; Zhang, X.; Xu, P.; Yuan, Q.; Samad, L.; Wang, X.; Wang, Y.; Zhang, Z.; Zhang, P.; Cao, X.; Song, B.; Jin, S. Contributions of Phase, Sulfur Vacancies, and Edges to the Hydrogen Evolution Reaction Catalytic Activity of Porous Molybdenum Disulfide Nanosheets. *J. Am. Chem. Soc.* **2016**, *138* (25), 7965−7972.

(190) Tan, Z. H.; Kong, X. Y.; Ng, B.-J.; Soo, H. S.; Mohamed, A. R.; Chai, S.-P. Recent Advances in Defect-Engineered Transition Metal Dichalcogenides for Enhanced Electrocatalytic Hydrogen Evolution: Perfecting Imperfections. *ACS Omega* **2023**, *8* (2), 1851−1863.

(191) Maiti, S.; Maiti, K.; Curnan, M. T.; Kim, K.; Noh, K.-J.; Han, J. W. Engineering electrocatalyst nanosurfaces to enrich the activity by inducing lattice strain. *Energy Environ. Sci.* **2021**, *14* (7), 3717−3756.

(192) Tao, L.; Lin, C.-Y.; Dou, S.; Feng, S.; Chen, D.; Liu, D.; Huo, J.; Xia, Z.; Wang, S. Creating coordinatively unsaturated metal sites in metal-organic-frameworks as efficient electrocatalysts for the oxygen evolution reaction: Insights into the active centers. *Nano Energy* **2017**, *41*, 417−425.

(193) Jia, C.; Sun, Q.; Liu, R.; Mao, G.; Maschmeyer, T.; Gooding, J. J.; Zhang, T.; Dai, L.; Zhao, C. Challenges and Opportunities for Single-Atom Electrocatalysts: From Lab-Scale Research to Potential Industry-Level Applications. *Adv. Mater.* **2024**, *36* (42), No. 2404659.

(194) Wang, Z.; Zhou, Y.; Qiu, P.; Xia, C.; Fang, W.; Jin, J.; Huang, L.; Deng, P.; Su, Y.; Crespo-Otero, R.; Tian, X.; You, B.; Guo, W.; Di Tommaso, D.; Pang, Y.; Ding, S.; Xia, B. Y. Advanced Catalyst Design and Reactor Configuration Upgrade in Electrochemical Carbon Dioxide Conversion. *Adv. Mater.* **2023**, *35* (52), No. 2303052.

(195) Deng, W.; Lee, A.; Dai, W.; Cherniack, L.; Crandall, B. S.; Li, H.; Jiao, F. Techno-economics of polymer-membrane-based CO_2 electrolysers. *Nat. Rev. Clean Technol.* **2025**, *1* (4), 255−268.

(196) He, R.; Xu, N.; Hasan, I. M. u.; Peng, L.; Li, L.; Huang, H.; Qiao, J. Advances in electrolyzer design and development for electrochemical CO_2 reduction. *EcoMat* **2023**, *5* (7), No. e12346.

(197) Ma, D.; Jin, T.; Xie, K.; Huang, H. An overview of flow cell architecture design and optimization for electrochemical CO_2 reduction. *J. Mater. Chem. A* **2021**, *9* (37), 20897−20918.

https://doi.org/10.1021/acs.est.5c06634
Environ. Sci. Technol. 2025, 59, 24177−24196

(198) Lv, H.; Wang, G. Solid oxide electrolysis cell for the super-dry reforming of methane. *Nat. Chem.* **2025**, *17* (5), 640−641.

(199) Koolen, C. D.; Pedersen, J. K.; Zijlstra, B.; Winzely, M.; Zhang, J.; Pfeiffer, T. V.; Vrijburg, W.; Li, M.; Agarwal, A.; Akbari, Z.; Kuddusi, Y.; Herranz, J.; Safonova, O. V.; Schmidt-Ott, A.; Luo, W.; Zuettel, A. Scalable synthesis of Cu-cluster catalysts via spark ablation for the electrochemical conversion of CO_2 to acetaldehyde. *Nat. Synth.* **2025**, *4* (3), 336−346.

(200) Wu, B.; Voleti, L. D.; Fenwick, A. Q.; Wu, C.; Zhang, J.; Ling, N.; Wang, M.; Jia, Y.; Tjiu, W. W.; Zhang, M.; Aabdin, Z.; Xi, S.; Mathpati, C. S.; Zhang, S.; Atwater, H. A.; Karimi, I. A.; Lum, Y. A reversed gas diffusion electrode enables collection of high purity gas products from CO_2 electroreduction. *EES Catal.* **2025**, *3* (2), 318−326.

(201) Wang, P.; Pei, A.; Chen, Z.; Sun, P.; Hu, C.; Wang, X.; Zheng, N.; Chen, G. Integrated system for electrolyte recovery, product separation, and CO_2 capture in CO_2 reduction. *Nat. Commun.* **2025**, *16* (1), 731.

(202) De Luna, P.; Hahn, C.; Higgins, D.; Jaffer, S. A.; Jaramillo, T. F.; Sargent, E. H. What would it take for renewably powered electrosynthesis to displace petrochemical processes? *Science* **2019**, *364* (6438), No. eaav3506.

(203) Bian, J.; Sun, C. Piezotronic-enhanced oxygen evolution reaction enabled by a Au/MoS_2 nanosheet catalyst. *Catal. Sci. Technol.* **2020**, *10* (18), 6180−6187.

(204) Zhang, P.; Zhu, P.; Zhang, F.; Wang, Y.; Zheng, W.; Liu, D.; Mao, Y. Enhanced electrocatalytic hydrogen evolution performance of 2D few-layer WS_2 nanosheets via piezoelectric effects. *Inorg. Chem. Commun.* **2021**, *132*, No. 108822.

(205) Bagherzadeh Mostaghimi, A. H.; Al-Attas, T. A.; Kibria, M. G.; Siahrostami, S. A review on electrocatalytic oxidation of methane to oxygenates. *J. Mater. Chem. A* **2020**, *8* (31), 15575−15590.

(206) Qiao, J.; Liu, Y.; Hong, F.; Zhang, J. A review of catalysts for the electroreduction of carbon dioxide to produce low-carbon fuels. *Chem. Soc. Rev.* **2014**, *43* (2), 631−675.

(207) Li, Z.; Wu, Y.; Wang, H.; Wu, Z.; Wu, X. High-Efficiency Electrocatalytic Reduction of N_2O with Single-Atom Cu Supported on Nitrogen-Doped Carbon. *Environ. Sci. Technol.* **2024**, *58*, 8976.

https://doi.org/10.1021/acs.est.5c06634
Environ. Sci. Technol. 2025, 59, 24177−24196